ELECTRICAL CHARACTERISTICS OF POLYMER-BASED FIELD EFFECT TRANSISTORS

by

Xiaotang Lu

B.Sc., Nanjing University, 1988
M.A.Sc., Southeast University, 1991

A THESIS SUBMITTED IN PARTIAL FULFILLMENT OF THE REQUIREMENT FOR THE DEGREE OF MASTER OF APPLIED SCIENCE

in the school

of

Engineering Science

Simon Fraser University

August 1993

APPROVAL

Name: Xiaotang Lu

Degree: Master of Applied Science (Electrical Engineering)

Thesis Title: Electrical characteristics of Polymer-based field-effect transistors

Examining Committee:

Committee Chairman: Dr. J. Jones
School of Engineering Science, SFU

Senior Supervisor: _____
Dr. M. J. Deen
School of Engineering Science, SFU

Senior Supervisor: _____
Dr. S. Holdcroft
Department of Chemistry, SFU

Committee Member: _____
Dr. R.F. Frindt
Department of Physics, SFU

External Examiner: _____
Dr. A. Rawicz
Department of Engineering Science, SFU

Date Approved: October 14, 1993

PARTIAL COPYRIGHT LICENSE

I hereby grant to Simon Fraser University the right to lend my thesis, project or extended essay (the title of which is shown below) to users of the Simon Fraser University Library, and to make partial or single copies only for such users or in response to a request from the library of any other university, or other educational institution, on its own behalf or for one of its users. I further agree that permission for multiple copying of this work for scholarly purposes may be granted by me or the Dean of Graduate Studies. It is understood that copying or publication of this work for financial gain shall not be allowed without my written permission.

Title of Thesis/Project/Extended Essay

"Electrical Characteristics of Polymer-Based Field Effect Transistor"

Author:

(signature)

Xiaotang LU
(name)

October 15, 1993
(date)

ABSTRACT

With the rapid development of the semiconductor industry, marked by the increasing density and complexity of the semiconductor chip circuitry, more attention is being given to novel materials that will overcome the difficulties associated with traditional materials. Organic polymers offer a viable alternative to the traditional inorganic materials in many applications because of their extremely small size, abundance, diversity, ease of fabrication and potential cost benefits.

In this thesis, poly(3–hexylthiophene) was chosen as the semiconducting material under investigation. Electrical transport mechanisms, fabrication and electrical characterization of polymer MISFETs were studied. These MISFET were fabricated using conventional semiconductor processing technology, and excellent FET current–voltage characteristics were observed. Electrical parameters such as threshold voltage, mobility, conductivity, carrier concentration and transconductance were typical of π–conjugated polymer based MISFETs. A circuit model using these electrical parameters is proposed. SPICE simulation results were in good agreement with experimental data. High frequency capacitance–voltage measurements were also conducted to study carrier formation at the semiconductor surface.

It is shown that, unlike traditional semiconductor devices, excitations such as solitons, polarons and bipolarons dominate carrier transport behavior. The poly-

mer MISFETs operate by modulation of the accumulation layer at the semiconductor–insulator interface. Improvements of the electrical performance of polymer MISFETs was accomplished by reducing polymer impurity levels during synthesis, photolytic tuning of polymer film thickness, and passivation of the active polymer region by organic materials.

ACKNOWLEDGMENTS

It is a pleasure to express my deep appreciation to Dr. M.J. Deen and Dr. S.Holdcroft for their excellent work in supervising my thesis project and their patience in correcting my thesis. Also a sincere thanks to Mr. M.S.A. Abdou, who has done excellent job in polymer synthesis and chemical characterization in this research, and to Mr. Z. Xie, who has successfully fabricated polymer devices with good electrical performances. Their cooperation and help in my thesis work are greatly appreciated. Thanks also go to my colleagues Arya Raychaudhuri, Forrest Ma, Joseph Liang and Zhixin Yan. This research was supported by the Natural Sciences and Engineering Research Council (NSERC) of Canada, the Science Council of British Columbia (STDF-AGAR Grant) and the Center of System Science (CSS), Simon Fraser University.

TABLE OF CONTENTS

LIST OF FIGURES

LIST OF TABLES

LIST OF SYMBOLS

k — Boltzman constant (eV/T)

ϵ — dielectric constant (Q^2/Vcm)

σ — conductivity (S/cm)

μ — mobility (cm^2/Vs)

n — carrier concentration ($1/cm^3$)

ν_{hop} — hopping probability (Hz)

ν_{ph} — phonon frequency (Hz)

Δ — energy bandgap (eV)

E_F — Fermi energy (eV)

E_C — conduction band energy (eV)

E_V — valence band energy (eV)

n_i — intrinsic carrier concentration ($1/cm^3$)

N_A — acceptor dopant concentration ($1/cm^3$)

R_S — source contact resistance of MISFET (Ω)

R_D — drain contact resistance of MISFET (Ω)

R_B — bulk resistance of MISFET (Ω)

I_{DS} — source and drain current of MISFET (A)

V_{DS} — source and drain voltage of MISFET (V)

V_{GS} — gate and source voltage of MISFET (V)

I_{bk} — bulk current of MISFET (A)

I_{ch} — channel current of MISFET (A)

W — channel width (cm)

L — channel length (cm)

V_f — flat band potential (V)

V_T — threshold voltage of MISFET (V)

C_{ox} — Silicon oxide capacitance (F)

λ — channel length modulation coefficient (1/V)

g_m —transconductance of MISFET (S)

g_D — channel conductance of MISFET (S)

V_S — surface potential (V)

E_S — surface electric field (V/cm)

Chapter 1 Introduction

While it is expected that silicon-based technology will continue its dominance of the integrated circuit market, at least for the near term, other avenues must be explored in order to satisfy demands that cannot be easily accomplished with silicon. For examples, high speed optoelectronics circuits and microwave and millimeter wave circuits are now routinely fabricated with GaAs- and InP-based technologies; and high temperature electronics for which SiC and diamond are being researched as possible candidates.

As electronic and optoelectronic devices become increasingly complex, and the devices and materials from which they made are pushed to their limits, novel devices or devices utilizing novel materials are becoming increasingly attractive. In contrast to group IV materials (C, Si, Ge) or the group III-V materials (GaAs, InP, GaSb) which are inorganic materials, organic polymers which can be processed to possess electrical properties from highly insulating (resistivity $\sim 10^8 \Omega\ cm$) to highly conducting

(conductivity $\sim 10^5 S/cm$) are now under increasing research investigation [Yosh87,Tomo87,Garn87,Fich89,Tomo89,Glen89,Burr89,Koez87,Assa88,Horo91, Garn90,Tayl91] . The fact that they are organic materials means that they can be of extremely small size (order of molecular lengths), are abundant, and are relatively inexpensive.

The most promising class of organic materials are the π–conjugated polymers which were prepared in pure form only 15 years ago [Ito74,Chia78]. These materials are under intense investigation because they exhibit semiconductor properties in their neutral state and high electronic conductivity in the partially oxidized state. Thin flexible films of the semiconducting plastic can be prepared by simple spin-casting of polymer solutions affording simple fabrication of devices utilizing flexible films. Prototype devices based on π–conjugated polymers have been reported. They include polymer/metal Schottky barrier devices [Yosh87,Tomo87,Garn87,Fich89,Tomo89,Glen89], field effect transistors [Burr89,Koez87,Assa88,Horo91,Garn90,Tayl91]. Recently elelectroluminescence from conjugated polymers was reported from which luminescent displays can be realized [Burr90].

The advantage of simplicity of fabrication must be weighed against the electronic inferiority of current plastics. However, the semiconducting properties of these materials have only just been realized and there is great optimism that electronic properties can be improved dramatically by chemical modification. Clearly,

tailoring electrical properties of polymer semiconductors can only be achieved by a thorough understanding of their molecular, microscopic and macroscopic properties. A detailed study of structure-property relationships as they pertain to microelectronic devices is therefore required.

Field effect transistors incorporating semiconducting organic polymers are useful devices for characterizing electrical parameters of these materials because they enable separation of the carrier generation and charge migration processes. π–conjugated materials studied by this technique include polyacetylene [Burr89], polythiophene [Yosh87,Koez87], oligothiophenes [Horo91,Garn90] and poly(3–alkylthiophenes) [Assa88,Tayl91]. Electrical characteristics are found to vary widely depending on the nature of polymer and the method of device fabrication. This reflects the embryonic nature of this research and the lack of understanding of structure-property, and morphology-property relationships.

In this thesis, the π–conjugated polymer, poly(3–hexylthiophene), is chosen as the semiconducting material under investigation. MISFETs incorporating this polymer are made using conventional MOS technology. A processing procedure has been customized in order to fabricate these plastics devices. The current–voltage measurements were performed with a probe station and automated semiconductor parameter analyzer. Excellent FET characteristics were observed and important FET electrical parameters were extracted. We also proposed an equivalent circuit model for SPICE simulations of these polymer-MISFETs.

The simulated results are in satisfactory agreement with experiment results for polymer-MISFET. In addition, high frequency capacitance–voltage measurements were carried out and a simple physical model was proposed to explain the unusual capacitive responses.

Based on the electrical transport mechanism reviewed in this thesis, several experiments were conducted on the polymer-MISFET structure. The motivation for doing these experiments was to improve polymer-MISFET performances by simultaneously increasing the effective mobility of carriers, device performance and environment stability.

MISFETs incorporating polymers of different purities were fabricated. The different current-voltage responses suggested that MISFETs based on polymers of low impurity concentration possessed high mobility, conductivity and thus are most suitable for FET devices. In a separate study a laser source was used to render the top layers of polymer-MISFET insulating. By doing this, the bulk ohmic current was suppressed and FET characteristics sharpened. Conducting polymers are very sensitive to ambient air and light. In order to prolong the lifetime of polymer-MISFETs by protecting them from the environment, a layer of conventional photoresist was used in to cover active polymer region. The electrical characteristics of these encapsulated FETs were monitored over 2 months. The stability of polymer MISFETs was greatly increased compared to devices exposed to ambient atmosphere.

Chapter 2 Carrier Transport Mechanisms in Conducting Polymers

Polymers are not traditionally associated with high electronic mobilities, but the rapid development of π–conjugated polymers as conductors and semiconductors has become the focus of attention during the past two decades. These materials depend on the presence of a delocalized and extended π–electron system, in which there is a p_z orbital on each carbon along the polymer backbone. This implies the possibility of metallic conductivity, but the instability of electrons energy state leads to single/double bond alternation of successive sites along the chain, thereby lowering the energy of the occupied states. This class of organic semiconductors exhibits a range of energy gaps (1.0 – 3.0eV) between the π valence band and the π^* conduction band.

Conducting polymers are quasi-one-dimensional materials. As a result of strong intrachain π–bonding, and relatively weak interchain electron transfer interaction, carrier transport along the polymer chain occurs with high mo-

bility. Carriers transport between the polymer chains is comparatively slow and these processes are the rate-limiting steps in three-dimensional transport. Anisotropic conductivity behavior has been reported in many conducting polymers [Kive81,Assa88,Wang86].

Understanding the transport properties in conducting polymers is one of the main goals in this field. It is commonly recognized that carriers in conducting polymers transport by thermal-assisted hopping between carbon sites, however, the interpretation of carrier transport data is still unclear, since transport properties are sensitive to structural defects and experimental data can not be interpreted unambiguously in terms of specific models.

2.1 Conducting Polymers

π–conjugated polymers, as prepared, are p-type semiconductors in their neutral form due to extrinsic carriers which arise from catalyst residue. The conductivity can be changed considerably (by a factor of 10^9) by chemical doping and undoping [Chia77], but the behavior is unlike conventional semiconductors doped with donors and acceptors. This doping process is reversible by injection and withdrawal of electrons electrochemically (Figure 2.1.1). The actual polymer structure and dopant content is very sensitive to the conditions of synthesis. Hence the system is much more complicated than Si, Ge and GaAs.

In addition to their chemical difference from traditional inorganic semiconduc-

tors, π–conjugated polymers are exemplified by the parent π–conjugated polymer, polyacetylene, and are physically characterized by the following features:

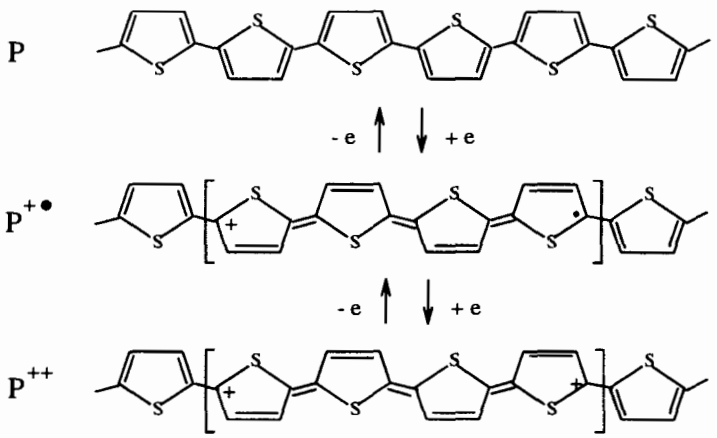

Figure 2.1.1 Schematic representation of reversible chemical doping and undoping of polythiophene.

1) The optical absorption of polyacetylene can be considered to possess a bandgap in its neutral form. Upon doping, additional infrared absorption peaks appear, which are associated with transitions of sub-levels in gap region to conduction band and valence band. Moreover, these absorption energies are independent of dopant concentration [Suzu80].

2) Pure polyacetylene exhibits pure Curie paramagnetism, corresponding to roughly one spin per several thousand (CH) groups. However, the electrical conductivity of pristine polyacetylene is small ($< 10^{-8}$S/cm) [Wein79], which means that these spin defects have zero charge. The most striking fact is that Curie paramagnetism drops upon doping while conductivity goes up. It is difficult to explain these phenomena using the traditional semiconductor theory.

In order to explain this special behavior in conducting polymers, a soliton model was introduced in 1979 by Su, Schrieffer and Heeger [Suwp79], and independently by Rice [Rice79]. A polaron-type excitation was first observed by Su and Schrieffer in molecular-dynamic studies on discrete chains [Suwp80], and analytic solution for polaron was discussed by Brazovskii and Kivora [Braz81], and Campbell and Bishop [Camp81].

2.2 Soliton, Polaron and Bipolaron Excitation

Theoretical models of soliton, polaron and bipolaron excitation in conducting polymer were established by using the SSH (Su, Schriffer, Heeger) model for π–electron system [Suwp80].

A two-fold degenerate system, like polyacetylene, has two structural configurations of identical ground state energy (Figure 2.2.1a) [Gros74]. If an electron is introduced into the chain, it initially goes into the conduction band as shown in Figure 2.2.1b. The structural change associated with injection of electron in-

creases the elastic energy, and the distorted chain relaxes to a form which has a reversed sense of band alternation inside the chain (Figure 2.2.1d). Associated with this electron is the non-bonding π–state inside the gap (Figure 2.2.1c). This electron and the associated phase kink is called a "soliton"; in fact it is an electron bound state associated with a topological defect in the lattice configuration.

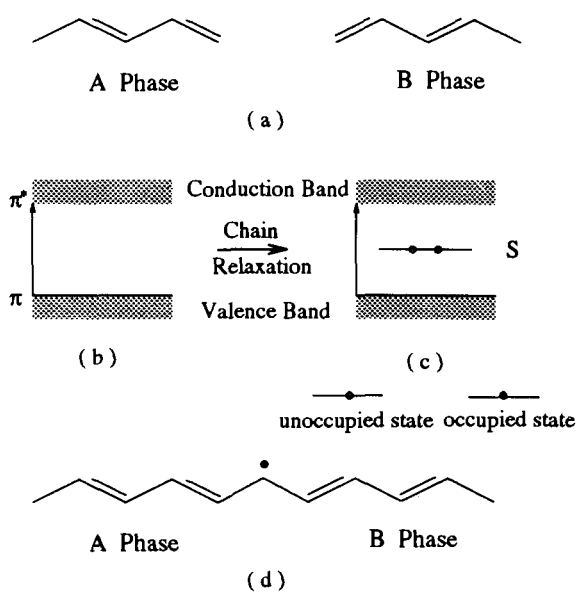

Figure 2.2.1 Schematic representation of the formation of a soliton on a polyacetylene chain
(a) undistorted chain with two structural configurations but degenerate ground state.
(b) when an electron is introduced onto chain.
(c) chain relaxation creates a soliton non-bonding state in the middle of gap.
(d) A reversed sense of bond alternation separated by a soliton.

Depending on the electron occupancy on the non-bonding π–state inside the bandgap, the soliton has three configurations with different charge and spin. Figure

2.2.2(a) shows that the neutral soliton S^0 has zero charge but spin 1/2; and when the electron is moved from non-bonding state, it posseses chrage +e but spin zero (Figure 2.2.2b); and when another electron is added to this state, it becomes charged –e and spin zero (Figure 2.2.2c). It is obvious that soliton has a special reversed spin-charge relation compared with electrons and holes.

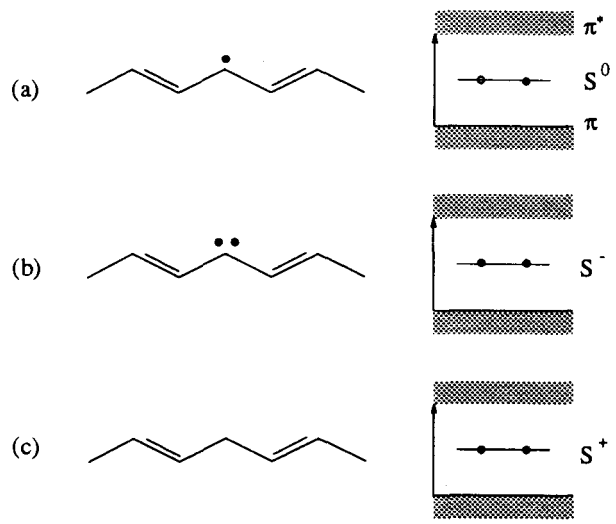

Figure 2.2.2 Schematic representation of three configurations of soliton excitation and the associated energy band diagram.

According to the SSH continuum model, in fact, the bond alternation defect is not localized at a single carbon site, but spreads over 10 to 15 carbon sites, with a correlation length ξ=7a (a is the distance between carbon sites) [Suwp79].

The soliton formation energy E_s is considered as follows:

a) The soliton resides in the middle of the energy bandgap, it is higher in energy than the top of the valence band by E_b.

b) The elastic energy is modified by ΔE_L.

c) The valence band spectrum is modified by ΔE_v.

Therefore,

$$E_s = E_b + \Delta E_v + \Delta E_L = \frac{1}{\pi}\Delta \qquad (2.2.1)$$

where Δ is the energy band gap of conducting polymer. The soliton creation energy is smaller than the electron and hole energy, hence storage of added charge on the mid-gap state is energetically favored over storage in bond states.

For non-degenerate systems like polythiophene, another popular family of conducting polymer under investigation (Figure 2.2.3a), the term "polaron" is used to denote a localized electron state with accompanying lattice distortion. It is a bound state of a soliton and anti-soliton pairs (one neutral and one charged, with centers separated by a sub–bandgap) [Barz81,Camp81], and it usually has two ground states E_+ and E_- inside the bandgap. Depending on the occupancy of two states, it can be classified as a "neutral polaron" (n_+=0 and n_-=2), a "hole" polaron (n_+=0 and n_-=1) or an "electron" polaron (n_+=1 and n_-=2) (Figure 2.2.3b). The formation of a hole polaron excitation is energetically more favored than the other two configurations.

The total energy of the polaron also consists of three parts: the bound state energy, the elastic energy, and the energy change of the extended state. The value of this energy is $\frac{\sqrt{2}}{\pi}\Delta$, which is larger than the creation energy of a single kink, but smaller than the electron and hole energy.

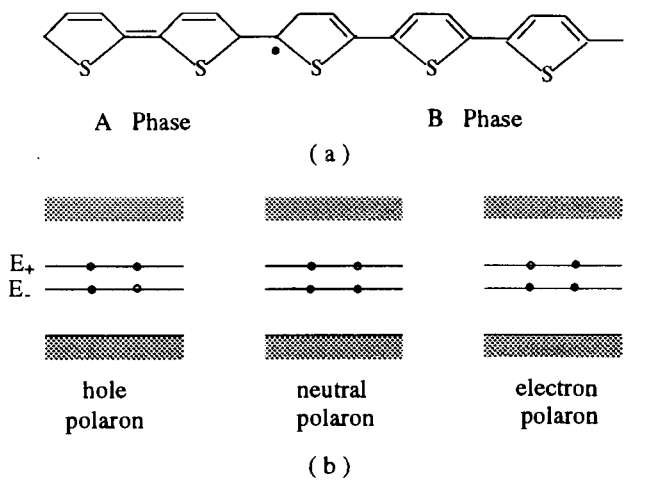

Figure 2.2.3 Schematic representation of polaron excitations in polythiophene. (a) polythiophene has two structural configurations but non-degenerate ground states. (b) Two polaron states exist inside bandgap with energy separated by a gap, depending on the electrons occupancy inside bandgap, it has three excitation forms.

For the non-degenerate system, the possibilities of $n_+=n_-=0,1,2$ give rise to "bipolaron" excitations. (Figure 2.2.4). The energy of a bipolaron is less than that of two polarons, $E_B < 2E_P$, so that the reaction

$$P^+ + P^+ \rightarrow B^{2+}$$

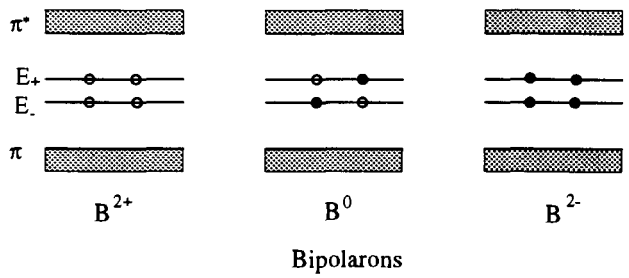

Figure 2.2.4 Schematic representation of three bipolaron excitations in polythiophene.

takes place. However both repulsive coulomb interactions and entropic forces favor the existence of the two separate polarons [Heeg 91]. Hence the free energy of creation of two polarons may be comparable to that of a bipolaron. Studies of polythiophene suggests that doping charges are stored in bipolaron states but small concentration of polarons can be expected.

2.3 Hopping Model for Carrier Transport

In conventional semiconductors, electrons and holes dominate transport. In conducting polymer, solitons, polarons and bipolarons dominate transport. Two conduction mechanisms are possible: hopping between localized states [Park 80]; and thermal excitation to the extended states [Suwp80].

For the conduction process to occur by hopping between localized states, the probability of hopping between sites of distance R is given by

$$\nu_{hop} = \nu_{ph} exp\left\{ -2\alpha R - \frac{W \pm eRE}{kT} \right\} \qquad (2.3.1)$$

where the component exp(-2αR) is due to the wave function overlap, W is the hopping barrier height, ν_{ph} is the frequency of phonons, and E is the external field.

For weak fields eRE << kT, the mobility is given as

$$\mu = \frac{2eR^2\nu_{ph}}{kT} exp\left(-2\alpha R - \frac{W}{kT} \right) \qquad (2.3.2)$$

From a topographical point of view, hopping can be classified as either intrachain or interchain. Townsend and Friend [Town87] consider that carriers hopping between polymer chains is the rate-limiting step for three-dimensional transport, since the hopping distance R and the hopping barrier W between chains are much larger those along the chain. Mobility is exponentially dependent on these two parameters: it decrease dramatically with the increment of R and W. Experimental observation shows that the room temperature conductivity of oriented polyacetylene along the direction of orientation is 3×10^{-5}S/cm, but the corresponding value for unoriented polyacetylene is 3×10^{-8}S/cm, i.e., 1000 times lower [Town87]. The enhancement of conductivity along the oriented samples arises from the evidence that carriers in oriented samples are more likely to hop along the chain, and less interchain hopping is expected compared with unoriented sample.

In a conduction process which involve thermal exciation to the extended states, e.g., like in conventional semiconductor, the d.c. conductivity

$$\sigma \propto exp\left(-\frac{E_c - E_F}{kT}\right) \qquad (2.3.3)$$

The temperature dependence of the resistivity [Town87] indicates that carriers generation is thermally activated, with activation energies corresponding to difference in energy between bandgap states to conduction band.

It is well known that carriers mobilities in chemically doped polyacetylene can reach the metal regime [Base87], this transition of mobilities by chemical doping is the characteristics of the hopping transport, where the cooperative effects of high concentration of charges greatly reduce the interchain hopping distance and hopping barriers energy. If dopant species A is represented in polymer chain as $[(CH)A_y]_x$, as y is changed from 0.001 to 0.01, there is a large increase in mobility. This is loosely described as the transition from semiconducting to metallic behavior, but a detailed model for the electronic structure at these dopant concentration is not well established.

2.4 Current-Voltage Characteristics of Conducting Polymers

For conducting polymers, current arises mainly from carrier drift under an applied electric field. The diffusive contribution to the total current is relatively small [Mark62]. Therefore the current density is related to applied voltage by

$$J = ne\mu E = \frac{ne\mu V}{d} = \frac{\sigma V}{d} \qquad (2.4.2)$$

where V is the applied voltage and d is the distance between electrodes.

Using a weak field approximation, the hopping model predicts a mobility, thus conductivity, which is independent of applied electrical field, or any parameters related to the geometry. The current at this region can be expressed as linear function of the applied voltage, i.e., ohmic current.

Under increasing electric field, charge unbalance is produced by the injection of electrons/holes through ohmic contact. Since the polymer has a relatively low density of free carriers, the current flow through polymer becomes limited by space charges.

The space charge density for an ohmic contact is formulated as

$$n = \frac{\epsilon\epsilon_0 V}{ed^2} \qquad (2.4.3)$$

and the space charge limited current (SCLC) density as

$$j = \frac{\mu\epsilon\epsilon_0 V^2}{d^3} \qquad (2.4.4)$$

A typical J-V curve for conducting polymer is plotted in Figure 2.4.1 on logarithmic scale [Xuba91]. The ohmic current is proportional to voltage while the SCLC is proportional to the voltage squared. The current changes from ohmic to space charge limited at

$$V = \frac{ned^2}{\epsilon\epsilon_0} \qquad (2.4.5)$$

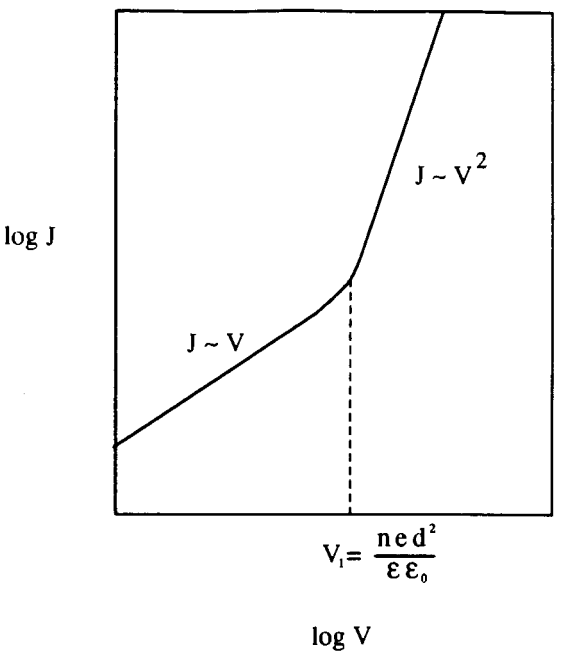

Figure 2.4.1 Current-voltage relationship for semiconducting polymer: ohmic current for small applied voltage, space-charge-limited current for high voltage.

From the polymer J-V curve, the mobility can be determined at SCLC region, and conductivity can be obtained from ohmic current at low voltage. Results of mobility and conductivity value extracted from J-V are reported to be in good agreement with results by the other methods [Garn89].

Chapter 3 Review of MIS Structures and MISFETs

In this chapter, basic concepts and mechanisms of silicon MIS structures and MISFETs are reviewed in order to compare with the electrical characteristics of polymer-based MIS structures and MISFETs.

3.1 The MIS Structure and Its C-V Characteristics

The metal-insulator-semiconductor (MIS) structure is a useful device for studying the semiconductor surface, since reliability, stability and device operation are intimately related to the surface conditions. A typical silicon MIS structure is shown in Figure 3.1.1.

The energy-band diagram of an ideal MIS structure for a p-type substrate is shown in Figure 3.1.2. When an ideal MIS structure is biased with positive or negative voltages, three situations may exist at the semiconductor surface. When a negative voltage ($V<0$) is applied to the metal contact, the top of the valence band

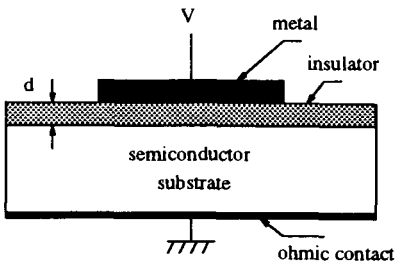

Figure 3.1.1 A typical Si MIS structure.

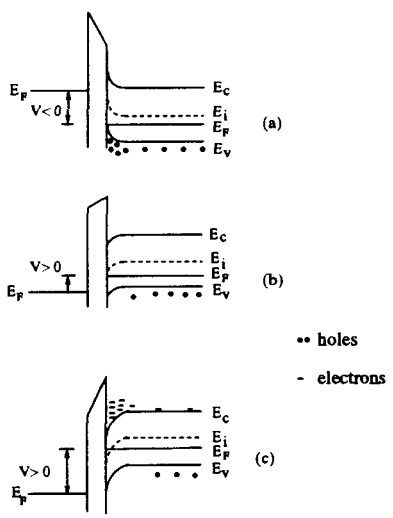

Figure 3.1.2 The energy-band diagram of an ideal MIS structure for a p-type Si substrate. (a) accumulation region; (b) depletion region; (c) inversion region.

bends upwards towards the Fermi level, while Fermi level remains constant (Figure 3.1.2a). This band bending causes an accumulation of majority carriers

(holes) near the semiconductor surface. This is the "accumulation" case. When a small positive voltage (V>0) is applied, the bands bend downward, and the majority carriers are depleted from the surface (Figure 3.1.2b). This is the "depletion" case. When a large positive voltage is applied, the bands bend downward to a higher degree so that the intrinsic level E_i at the surface crosses over the Fermi level E_F (Figure 3.1.2c). At this point, the number of minority carriers (electrons) at the surface is larger than that of the holes, the surface is thus inverted; the so-called "inversion" layer.

This voltage dependency is reflected in capacitance-voltage (C-V) curves. A typical p-type silicon C-V curve is shown in Figure 3.1.3. At negative voltage, high differential capacitance exists due to the accumulation of holes at polymer/insulator interface. As a result the total capacitance is virtually the same as the insulator capacitance. When the negative voltage is sufficiently reduced, a depletion region is formed which act as a dielectric layer in series with the insulator. The total capacitance decreases and shows a minimum capacitance, C_{min}, which corresponds to the maximum depletion depth, W_m.

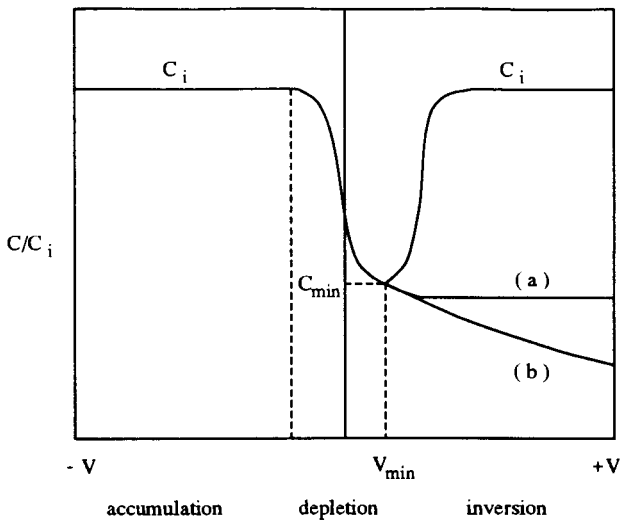

Figure 3.1.3 Capacitance-Voltage responses for a Si p-type MIS structure.

$$C_{min} = \frac{C_i C_{D,max}}{C_i + C_{D,max}} \tag{3.1.1}$$

$$C_{D,max} = \frac{\epsilon\epsilon_0 S}{W_m} \tag{3.1.2}$$

where

$$W_m = \sqrt{\frac{4\epsilon kT ln\left(\frac{N_A}{n_i}\right)}{q^2 N_A}} \tag{3.1.3}$$

and S is gate region area, ϵ is dielectric constant, N_A is acceptor dopant concentration and n_i is intrinsic carrier concentration. It can be easily seen from the above equation, the extrinsic carrier concentration N_A can be deduced from the minimum capacitance value.

As the voltage is made more positive, the capacitance increases again as the inversion layer of electrons forms at the surface. Finally, a value close to insulator capacitance is obtained. Note that the increase of the capacitance in the latter region depends on the ability of the electrons to follow the applied a.c. signal. This occurs only at low frequencies where the rates of recombination-generation of minority carriers can keep up with the small-signal variation and lead to charge exchange with the inversion layer in step with the measurement signal. It is experimentally found that for metal-SiO_2–Si system the frequency must be between 5–100 Hz in order to observe the inverted region [Sze81]. As a consequence, C-V of MIS structures measured at high frequency does not show the increase of capacitance at high positive voltage. Figure 3.1.3 shows two cases for measurements made at high positive voltages: In case (a), the minority carriers can not be supplied to and extracted from the oxide/silicon interface rapidly enough (by diffusion or generation-recombination) to respond to the signal voltage variation at high frequency. Instead a steady-state concentration of the minority carriers is accumulated at the Si-SiO_2 surface. Case (b) is called "deep depletion", because the d.c. voltage sweep is so rapid that the minority carriers can not be accumulated at the oxide/silicon interface, or are generated so slowly that few are generated and accumulated at the gated Si surface before the C-V trace is completed, the depletion layer thickness increases with the applied gate voltage and no minimum capacitance is reached in this case.

3.2 The MOSFET and Its I-V Characteristics

The metal-oxide-semiconductor field-effect transistor (MISFET or MOSFET) is the basic device for digital circuitry and is widely used in very large scale integrated circuits such as microprocessors and semiconductor memories. The basic structure of an n–channel silicon MOSFET is illustrated in Figure 3.2.1.

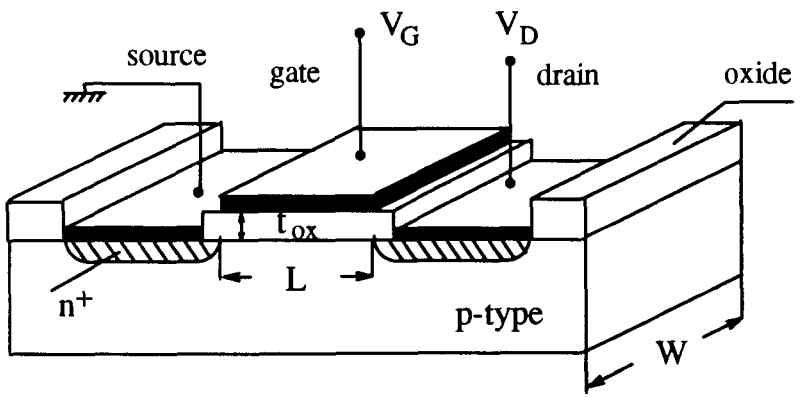

Figure 3.2.1 Basic structure of Si n-channel MOSFET.

It is a three-terminal device and consists of a p-type semiconductor substrate with two heavily doped n^+ regions, the source and drain. The metal contact on the insulator is called gate. Heavily-doped polysilicon or a combination of silicide and polysilicon can also be used as the gate electrode. The basic device parameters

are the channel length L, the channel width W, the insulator capacitance C_{ox} for silicon oxide, and substrate carriers concentration N_A.

A qualitative discussion of device operation is presented: when no voltage is applied to the gate V_G=0, the source-to-drain electrodes correspond to two p-n junctions connected back to back. The only current that can flow from source to drain is the reverse leakage current. When a sufficiently large positive bias is applied to the gate so that a surface inversion layer is formed between two n^+ regions, the source and the drain are connected by a conducting channel for electrons, through which a large current can flow. If a small drain voltage is applied, the drain current I_D is proportional to the drain voltage V_D, since the channel acts only as a resistance. This is so called "linear region", Figure 3.2.2a. As the drain voltage increases to V_{Dsat}, the channel depth at drain end is reduced to zero, and is called pinch-off point (Figure 3.2.2b). When V_D is made larger than the saturation voltage V_{Dsat}, the pinch-off point moves towards source end and the voltage at this point remains the same, V_{Dsat}. Hence the current flow from the source keeps constant, and beyond this pinch-off point, the carriers are drifted by the applied electric field along the channel direction, the drain current remains essentially constant. It can be noticed that the effective channel length decreases from L to L', Figure 3.2.2c.

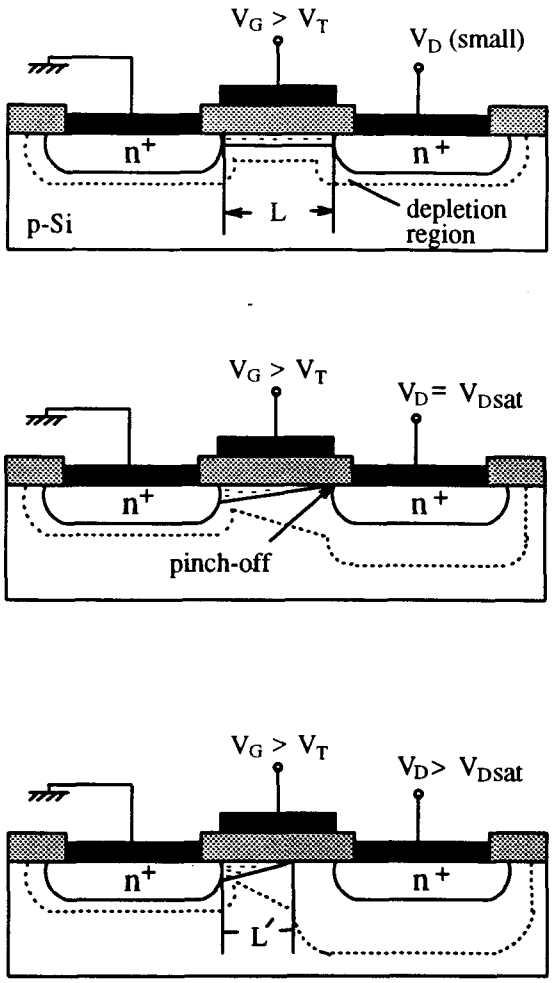

Figure 3.2.2 A schematic representation of MOSFET operation.

The basic current-voltage characteristics of a MOSFET can be derived as follows.

For the linear region:

$$I_D = \mu C_{ox} \frac{W}{L} \left((V_G - V_T) V_D - \frac{1}{2} V_D^2 \right) \qquad for\ V_D < V_G - V_T \quad (3.2.1)$$

and for the saturation region:

$$I_D = \frac{1}{2} \mu C_{ox} \frac{W}{L} (V_G - V_T)^2 (1 + \lambda V_D) \qquad for\ V_D \geq V_G - V_T \quad (3.2.2)$$

where V_T is the threshold voltage for the formation of inversion channel layer, and λ is called channel length modulation coefficient and is related to the effective channel length.

The transconductance g_m and the channel conductance g_D are defined as:

$$g_m = \frac{\partial I_D}{\partial V_G} \qquad for\ \ constant\ \ V_D$$

$$= \begin{cases} \mu C_{ox} \frac{W}{L} V_D & linear\ region \\ \mu C_{ox} \frac{W}{L} (V_G - V_T) & saturation\ region \end{cases}$$

$$g_D = \frac{\partial I_D}{\partial V_D} \qquad for\ constant\ V_G$$

$$= \begin{cases} \mu C_{ox} \frac{W}{L} (V_G - V_T - V_D) & linear\ region \\ \mu \lambda C_{ox} \frac{W}{L} (V_G - V_T)^2 / 2 & saturation\ region \end{cases}$$

Chapter 4 Electrical Characteristics of Polymer-MISFETs

In this chapter, synthesis of poly(3–hexylthiophene) (prepared in the Department of Chemistry), and MISFET and MIS device fabrication are described. Current-voltage characteristics of thin film polymer MISFETs are investigated. Important electrical parameters such as mobility, conductivity, threshold voltage, transconductance and channel conductance have been extracted. A equivalent circuit model is proposed for SPICE simulation, the simulation results based on this model are shown to have good agreement with experimental data. Capacitance-voltage characteristics of a polymer-MIS structure were also studied. The latter shows formation of accumulation layer and depletion layer at the polymer semiconductor surface. A simple physical model is established to explain capacitance behavior of this structure.

4.1 Synthesis of Poly(3–hexylthiophene)

Poly(3–hexylthiophene), a derivative of intractable polythiophene has been chosen as the material under research. This materials was synthesized and characterized by M.S.A. Abdou of Department of Chemistry, Simon Fraser University. Derivatization of the 3–position of the thienyl ring with long alkyl chains imparts solubility, and thus processability, yet adjacent rings maintain coplanarity. Thus the polymer exhibits extensive π–conjugation, and possess the desirable electronic and optical attributes of unsubstituted polythiophenes. They have advantage of being spin-cast in addition to rigorous chemical characterization.

The synthesis of poly(3–hexylthiophene) (Figure 4.1.1) is as follows:

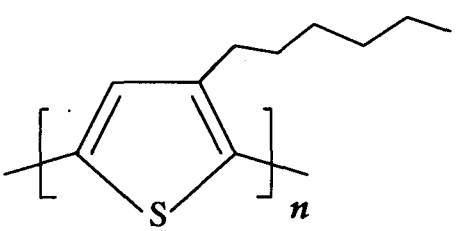

Figure 4.1.1 Chemical structure of Poly(3–hexylthiophene).

3–Hexylthiophene was synthesized by coupling the Grignard reagent of 3–bromothiophene (Aldrich) with 1 bromohexane using bis(1,3–diphenylphosphino)

propane nickel(II) chloride as catalyst. The product was purified by fractional distillation under reduced pressure. Polymerization of the monomer was achieved by mixing 0.1 M solution of 3–hexylthiophene in chloroform with a 0.4 M chloroform solution of anhydrous ferric chloride. The mixture was stirred for two hours prior to precipitation into acidified methanol. The solid product was filtered, washed with NH_4OH, water and methanol. The crude polymer was dissolved in hot dichloromethane and insoluble products were removed by filtration. Low molecular weight products were removed by cooling the filtrate and adding methanol. The precipitate was filtered and dried in a vacuum oven. The number average molecular weight of the polymer was 26,200 as determined by size exclusion chromatography [Hold91–3].

4.2 Fabrication of Devices

Polymer device fabrication requires the successive deposition of insulator, metal and polymer, with appropriate patterns for the device structures. Silicon was chosen as the support substrate in polymer devices, because it can be heavily doped to form a gate electrode, and it can be easily thermally oxidized into silicon oxide insluator layer. The Si substrate, however, plays no active role in the devices operation. Silicon dioxide has excellent insulating properties with low defect density, relatively high dielectric constant ϵ_r and a high dielectric breakdown field E_b. It is extensively used in polymer device fabrication. Gold

was evaporated onto the substrate for source and drain contacts. Gold forms ohmic contact with the polymer [Burr89, Garn90].

A schematic representation of the polymer–MISFET used in this study is shown in Figure 4.2.1.

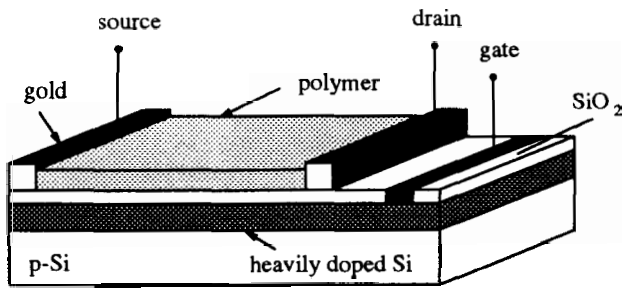

(a)

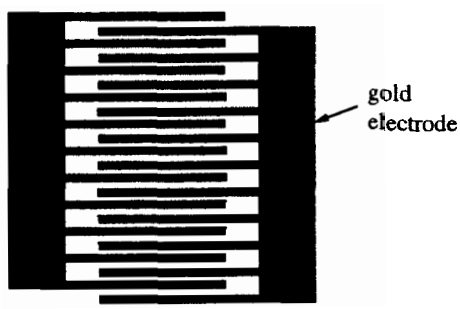

(b)

Figure 4.2.1. (a) A schematic representation of polymer-MISFET.
(b) Actual pattern of source and drain contact.

Silicon is used as a substrate, a heavily doped Si layer served as the gate and a thermally grown oxide layer is employed as the insulator. Two inter-digital

structures of gold were deposited photolithographically on top of the insulator and used as source and drain. The polymer semiconductor layer was spun on the structure to form working devices. The detailed description of fabrication process is given below and shown in Figure 4.2.2.

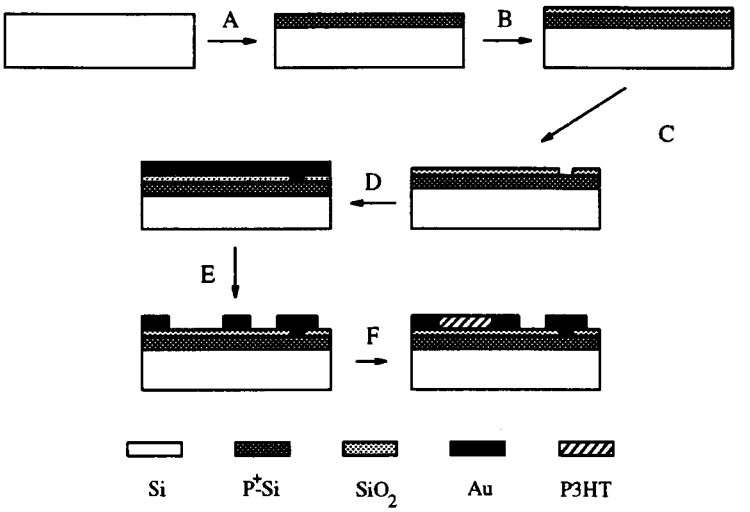

Figure 4.2.2. Fabrication scheme for polymer-MISFET.

A. The starting substrate is a 3", <100> oriented n/p-type silicon wafer. After performing standard degrease and clean procedures, dopant source was spun on the wafer. Thermal diffusion of dopants was carried out at 1100°C with N_2 flow and O_2 flow. The heavily doped layer served as gate for polymer–FET structure.

B. A layer of silicon oxide (200nm) is grown by a combination of dry and wet oxidation procedures at 1100°C.

C. AZ 1312SFD photoresist was used to perform laser direct writing photolithography on the oxide layer in order to open connection windows. The treatment procedures for photolithography are: spin casting and baking of photoresist at 95°C for 0.5hr; exposed to blue laser light; developed by AZ developer, and postbaking at 120°C for 0.5hr.

D. A 20 nm layer of gold was vacuum evaporated onto the substrate.

E. AZ 1312SFD photoresist was used again and one hundred gold fingers of width 10 μm and length 300 μm and spaced 14μm apart are patterned photolithographically.

F. Photolithography was used to pattern the photoresist to expose an active region. Dilute polymer solution was spun on the wafer at 7000 rpm (film thickness $\sim$0.25μm). The photoresist was lifted off by immersion into solvent for photoresist.

Figure 4.2.3 shows the MIS structure used in our capacitance-voltage measurements. MIS structures were also fabricated on a silicon wafer substrate, with silicon oxide as the insulator, and a heavily doped silicon layer acting as one of the electrodes. A layer of aluminum was evaporated and patterned as contact pads. Polymer was cast onto the insulator ($\sim$1μm film thickness). On the top

of polymer, a layer of silver epoxy glue was applied and the structure was annealed in N_2 at 120°C for 1hr. Gold wires, bonded to one aluminum pad, were buried into silver paste for connection. The use of silver paste was preferred over metal evaporation, since the polymer structure can not withstand the high temperatures (500–700°C) associated with metal evaporation. This structure was able to be bonded to dual in-line package (DIP), and plugged into HP 16058 test fixture with good electrical and magnetic radiation shielding. The whole C-V measurements were conducted in a dark environment.

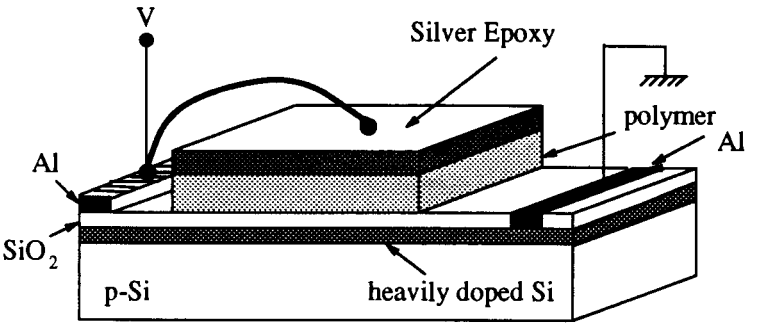

Figure4.2.3 Polymer-MIS structure for Capacitance-Voltage measurements

Around 100 polymer-MISFETs of 5 lots were fabricated in this study; 50–60 devices worked, and most of the failed devices were from structural defects due to gold fingers shorting. The polymer-MISFET in the same lot had identical

electrical performances, and electrical characteristics of polymer-MISFET from different lot were close. In the whole, the polymer-MISFET has good processing reproductivity and electrical behavior repeatability.

4.3 Measurement Techniques

An automated microelectronics measurement system has been implemented in this study. The hardware and software integrated measurement system is capable of taking measurements for current-voltage characterization and capacitance-voltage characterization.

The current-voltage characteristics of polymer MISFET's were measured with a semiconductor parameter analyzer HP4145 and a BAUSCH & LOMB wafer probing station. The measurement processes for test configuration, data flow control and acquisition were programmed and controlled by personnel computer incorporated with IOTech IEEE 488 drive board and software driver. In our experiments, I_{DS}–V_{DS} was measured to observe polymer FET-like characteristics; plots of I_{DS}–V_{GS} were to determine the gate bias modulation on the FET conductive channel; and I_{GS}–V_{GS} measurements provided information on the quality of the silicon oxide layer.

The capacitance-voltage characteristics of poly(3–hexylthiophene) were measured with Keithly series CV meter, the voltage sweep was varied from –20V to 20V and the a.c. frequency was 1MHz. The measurement parameters selec-

tion, data acquisition and analysis were controlled by Model82–DOS software. High frequency C-V results were utilized to study the formation of depletion and accumulation layers at different gate bias.

4.4 Polymer-MISFET I-V Characteristics

Prior to annealing the polymer-MISFETs, I_{DS}-V_{DS} curves of polymer-MISFETs showed a large resistive current, small gate bias modulation and an absence of a saturation region (Figure 4.4.1). This is primarily due to the presence of partially oxidized polymer which persists even after rigorous purification, these oxidized elements are mobile and contribute to the channel current under applied voltage. Scattering of carriers, arising from these oxidized elements, impedes the carrier transport through the channel and thus decreases the carrier mobility.

Thermal annealing at 180°C in N_2 is used to convert segments to their neutral form and thereby suppress ohmic contributions. It is well documented that oxidized and conductive polymer reverts to its neutral insulating state at elevated temperatures [Taka91, Wang91]. The phenomenon is due to thermal enhancement of the torsional angle between adjacent thienyl rings in the chain leading to unstable segments of high oxidation potential [Gran92].

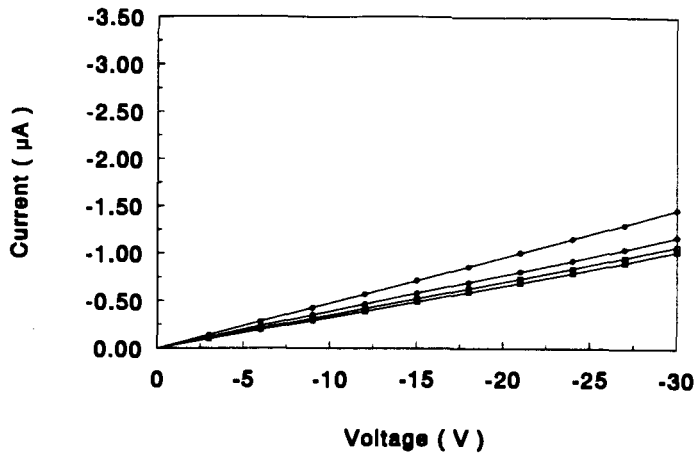

Figure 4.4.1 I_{DS}-V_{DS} characteristics of polymer-MISFET before annealing.

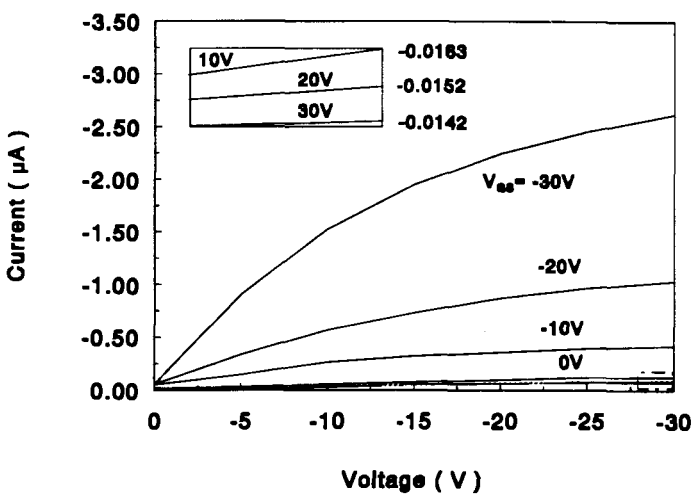

Figure 4.4.2 Typical I_{DS}–V_{DS} curves obtained for an annealed polymer MISFET with a thin film (0.25μm) semiconducting polymer substrate.

Figure 4.4.2 shows typical I_{DS}–V_{DS} curves obtained for an annealed polymer-MISFET with a thin semiconducting polymer film. As indicated in this figure, excellent FET-like behavior is observed with clear linear and saturation regions.

At negative gate biases, I_{DS} increases with V_{GS}, indicating that, unlike enhancement silicon MOSFETs, as-prepared p-type polymer-based thin film MISFETs operate through the modulation of accumulation layer at the semiconductor-insulator interface. It is assumed that negative gate biases attract majority carriers (e.g. positive bipolarons in P3HT) which accumulate at the polymer/insulator surface. With larger negative voltages, the carriers concentration at the surface is increased, therefore the current rises from the increment of carriers concentration.

It is well known that for enhancement p-type Si MOSFETs, when gate bias is zero, or below the threshold voltage, the equivalent circuit between source and drain ends is composed of two p-n diodes: one is forward biased, and the other is reverse biased. Current that flows through Si surface under these conditions is the leakage current of reverse diode, usually this current is negligible. Figure 4.4.2 shows that a considerable current exists at zero gate bias for polymer-MISFETs. The current is considered due to ohmic current that flows through bulk region of polymer, since no p-n diodes exist between the polymer substrate and both source and drain. Ohmic contacts at the source(drain)/polymer interface facilitates carrier drift under the applied source-drain voltage.

At positive gate biases, the carriers under the gate region are depleted from the insulator/polymer surface, and the polymer-MISFET works in depletion region, the total current arises mainly from the bulk current. As gate bias is made more positive, the depletion layer becomes thicker, while the bulk region becomes subsequently thinner, and thus the current flow through the bulk region decreases with the increased applied gate bias, but it does not show a considerable change with positive gate bias.

It is shown that total current in polymer MISFET can be separated into two currents: channel current and bulk current. Using established MOSFET and semiconductor current-voltage relationships, the channel current I_{ch}, can be formulated as

$$I_{ch} = \mu C_{ox} \frac{W}{L} \left\{ (V_{GS} - V_T) V_{DS} - \frac{1}{2} V_{DS}^2 \right\} \qquad (4.4.1)$$

and

$$I_{ch} = \frac{1}{2} \mu C_{ox} \frac{W}{L} (V_{GS} - V_T)^2 (1 + \lambda V_{DS}) \qquad (4.4.2)$$

for linear and saturation operation modes respectively, while bulk current I_{bk} can be represented as

$$I_{bk} = \frac{n\sigma W t_p}{L} V_{DS} \qquad (4.4.3)$$

where t_p is polymer layer thickness, L and W are channel length and width. The total current is equal to

$$I_{total} = I_{ch} + I_{bk} \qquad (4.4.4)$$

In our analysis of I_{DS}–V_{DS} responses of polymer–MISFETs, three assumptions are made:

(1) The current at zero gate bias is considered to be the ohmic current that flows through polymer substrate. The channel current below the threshold voltage is negligible compared with the bulk region current.

(2) Bulk current at negative gate biases is almost equal to that at zero gate bias. The accumulation layer thickness is comparatively much smaller than the polymer bulk thickness, therefore, the bulk region thickness does not show a considerable change.

(3) Mobility is considered to be weak function of gate biases, especially at low voltage range (0 to –30V).

Based on the above assumptions and equations, the conductivity can be determined from I_{DS}–V_{DS} at zero bias, which is approximately the bulk current (Equation 4.4.3). The bulk current is subtracted from currents at negative biases to determine the FET-like channel currents. Mobilities are determined using conventional MOS parameter extraction methods. We found it better to extract mobility from the linear region of the I-V plot rather than from saturation region, since the channel length modulation coefficient, λ (equation 4.4.2), at saturation region makes the calculation more complex and less accurate. The field effect mobility was determined to be $3.2 \times 10^{-5}\ cm^2V^{-1}s^{-1}$, the threshold voltage of

-1.2V and the conductivity of the polymer was $2.9 \times 10^{-7} S/cm$. The measured mobility is consistent with previous studies on poly(3–hexylthiophene). In comparison with other polythiophenes, the mobility is higher than 3–octyl and 3–dodecylderivatives ($10^{-6} \sim 10^{-7}\ cm^2V^{-1}s^{-1}$) [Palo91], but lower than 3–methyl and 3–butyl substituted analogues ($10^{-3} \sim 10^{-4}\ cm^2V^{-1}s^{-1}$) [Tayl91,Van91]. We attribute this to variations in crystallinity and interchain interactions which are more pronounced in short alkyl chain analogues. Based on the assumption that mobility is a weak function of gate bias at low voltage region, the majority carriers concentration can be estimated from

$$n = \frac{\sigma}{e\mu} = 5.7 \times 10^{16} cm^{-3}$$

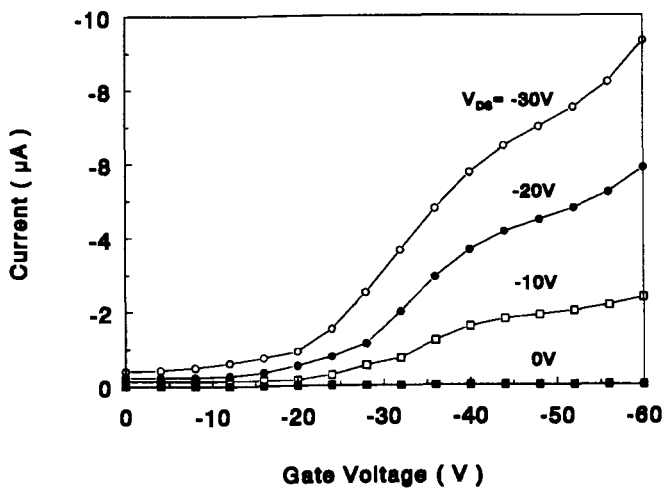

Figure 4.4.3 Typical I_{DS}–V_{GS} responses at different V_{DS} for an annealed polymer MISFET with a thin film (0.25μm) semiconducting polymer substrate.

I_{DS}–V_{GS} responses at different V_{DS} are shown in Figure 4.4.3. At zero gate bias, I_{DS} has a small current value, this is the bulk current at zero gate bias. For a small gate bias, I_{DS} increases linearly with V_{GS}. As V_{GS} is made more negative ($-20 \sim -40V$), I_{DS} shows a sharp increase, which corresponds to large gate biases modulation in the saturation region. At even higher gate biases (>-50V), current increment slows down. This is presumedly considered as the effect of surface scattering: At high gate bias, the carriers concentration at polymer/insulator surface is so large that the surface scattering, such as collision of carriers with insulator surface, becomes pronounced, therefore, mobility at this gate biases is comparatively lower than at small gate biases region.

Figure 4.4.3 is replotted as $\sqrt{I_{DS}}$ *versus* V_{GS} at V_{DS}=V_{GS} (Figure 4.4.4), a voltage condition that ensures MISFET is operating in the saturation region. From the intercept with voltage axis, a threshold voltage of –1 V is obtained, and from the gradient of this plot, we obtained a mobility of $3.5 \times 10^{-5}cm^2V^{-1}s^{-1}$. The discrepancy of mobilities extracted from two methods, i.e., I_{DS}–V_{DS} characteristics and $\sqrt{I_{DS}}$ *versus* V_{GS}, arises from the channel length modulation coefficient λ, in fact the mobility value obtained from $\sqrt{I_{DS}} - V_{GS}$ curve is actually equal to $\mu(1 + \lambda V_{DS})$. The λ for this device was found to be $5.0 \times 10^{-3}V^{-1}$.

Transconductance g_m is obtained from I_{DS} versus V_{GS} plot (Figure 4.4.2)and channel conductance g_D is obtained from the derivative of I_{DS} versus and V_{DS}

plot (Figure 4.4.3). Figures 4.4.5 shows the variation of g_m with V_{GS} at different

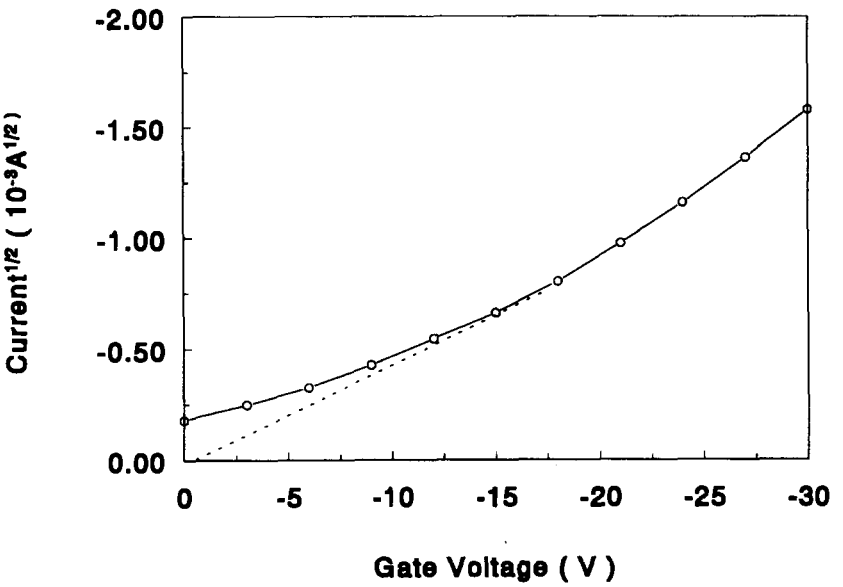

Figure 4.4.4 $\sqrt{I_{DS}} - V_{GS}$ curve at V_{DS}=V_{GS} for an annealed polymer MISFET with a thin film (0.25μm) semiconducting polymer substrate.

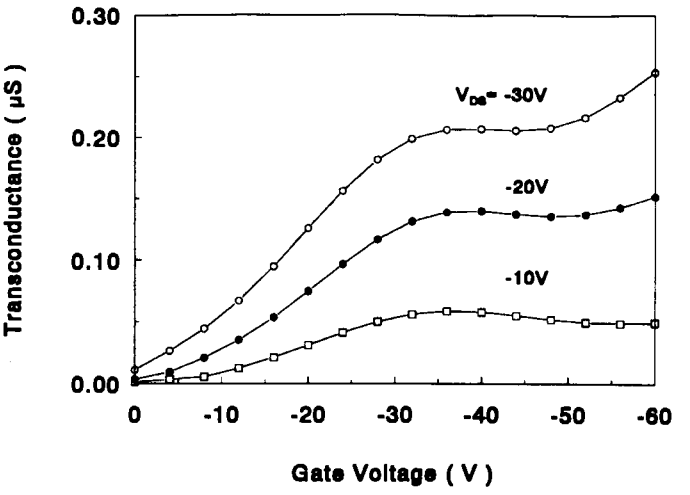

Figures 4.4.5 Variation of g_m with V_{GS} at different V_{DS}.

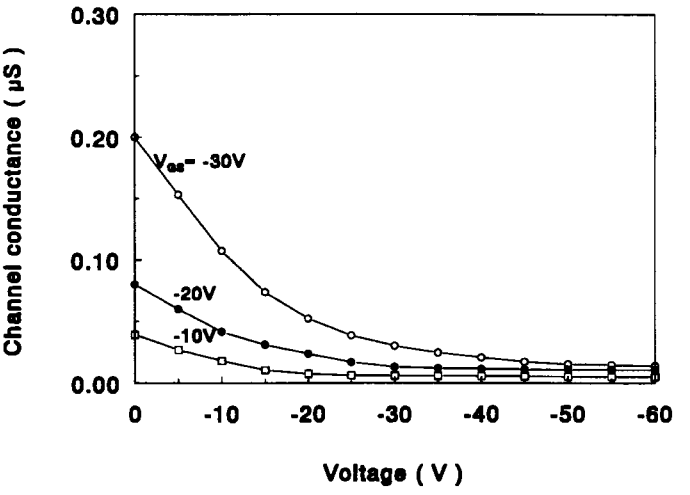

Figures 4.4.6 Variation of g_D with V_{DS} at different V_{GS} biases.

values of V_{DS}. Figures 4.4.6 shows the variation of g_D with V_{DS} at different V_{GS} biases. These characteristics are similar to those observed for silicon MOSFETs, except that they are several orders smaller in magnitude.

4.5 SPICE Model for Polymer-MISFETs

According to current-voltage characteristics in the polymer-MISFETs, we propose an equivalent circuit model (Figure 4.5.1). The channel region is treated as an enhancement mode PMOS transistor, and the bulk region as a resistor. We also consider the contact resistances at source and drain, which may related to poor formation of the gold-polymer contact. Using electrical parameters such as mobility, threshold voltage and zero bias resistance from experimental data, we have used the SPICE (Simulation Program with Integrated Circuit Emphasis) model to simulate I_{DS}–V_{DS} curves of polymer MISFETs.

The current-voltage relationships in Figure 4.5.1 are represented as:

$$V_{DS} = V_{ds} + I_{DS}(R_S + R_D) \qquad (3.5.1)$$

$$V_{GS} = V_{gs} + I_{DS}R_S \qquad (3.5.2)$$

$$I_{DS} = I_{FET}(V_{ds}, V_{gs}) + \frac{V_{ds}}{R_B} \qquad (3.5.3)$$

where R_D, R_S and R_B are drain contact resistance, source contact resistance and bulk region resistance respectively. In our simulation process, we choose a contact resistance of $\sim$1KΩ, and bulk resistance which varies with polymer thickness.

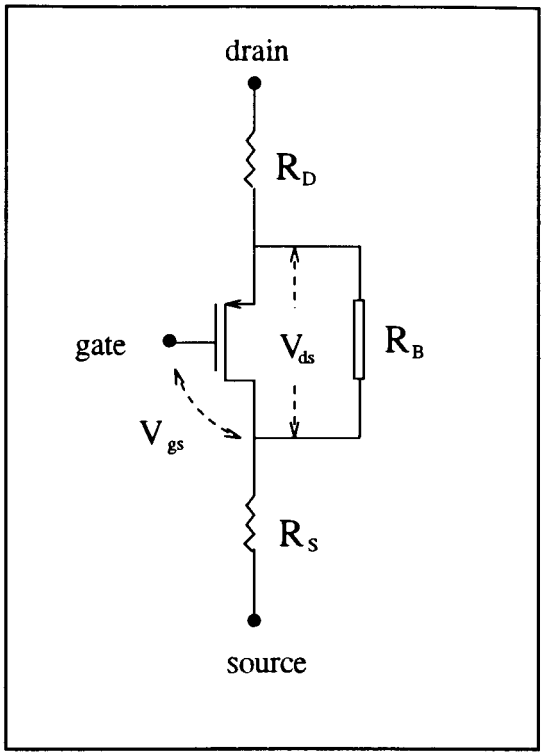

Figure 4.5.1 Equivalent circuit for the polymer-MISFET.

The SPICE simulation results for polymer film thickness of 0.25μm and 1μm are shown as solid lines in Figure 4.5.2 and Figure 4.5.3. Actual experimental I_{DS}–V_{DS} response are shown as dashed lines in the corresponding graph. Good agreements between simulated and experimental results are obtained, indicating

that the model shown in Figure 4.5.1 is a good circuit representation of the polymer MISFET. The Appendixes contains listings of SPICE decks used for the simulations.

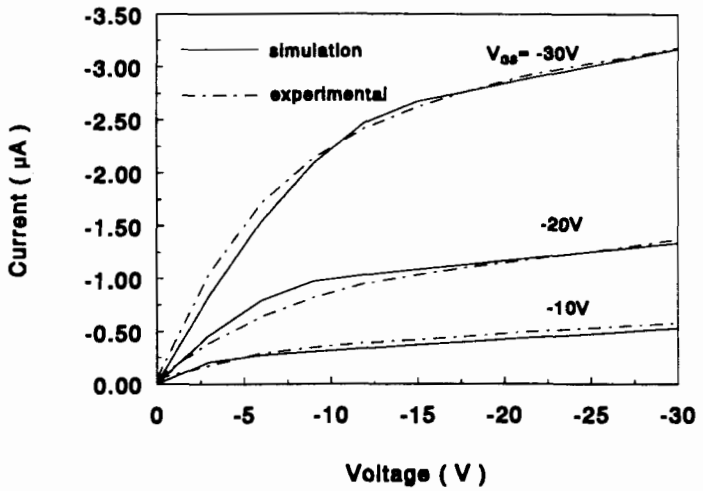

Figure 4.5.2 SPICE simulation results for I_{DS}–V_{DS} characteristics of polymer MISFETs with film thickness of 0.25μm. Experimental I_{DS}–V_{DS} response are shown as dashed lines in graph.

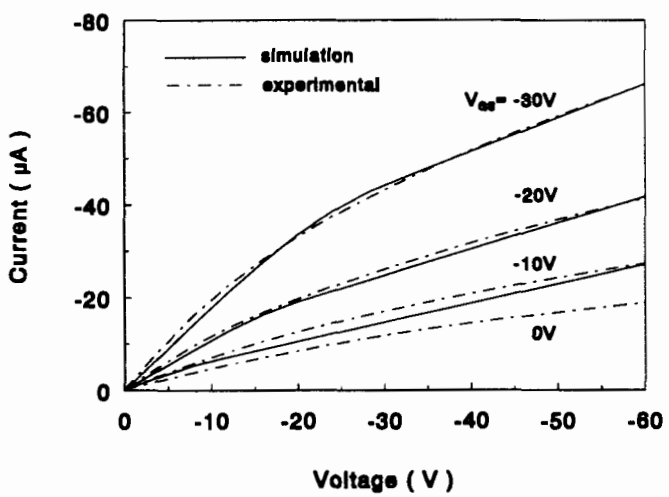

Figure 4.5.3 SPICE simulation results for I_{DS}–V_{DS} characteristics of polymer MISFETs with film thickness of 1μm. Experimental I_{DS}–V_{DS} response are shown as dashed lines in graph.

4.6 C–V Characteristics for Polymer–based MIS Structure

The capacitance of polymer MIS structure was tested under high frequency of 1MHz. The d.c. voltage was ramped from –20V to 20V at a rate of 2V/min. We chose a high frequency and slow sweep rate, since the carriers in the polymer might require a long relaxation time to reach equilibrium. A high a.c. signal might exclude the influence of mobile elements residing in polymer.

Electrical characterization of the MIS device is restricted to the measurement of the complex impedance. The equivalent circuit is shown in Figure 4.6.1,

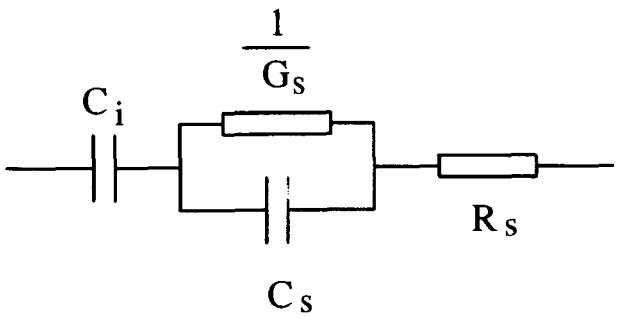

Figure 4.6.1. The schematic representation of equivalent circuit of polymer MIS structure.

and it can be considered as a series circuit of the insulator capacitance C_i and the semiconductor impedance (capacitance C_s, conductance G_s and series

resistance R_s). Series resistances equal to thick polymer film bulk resistance were compensated in our C-V results and the values of the compensated series resistance ranged from 30kΩ to 100kΩ. The relationships of series resistance compensated capacitance C_c with the measured capacitance C_M and conductance G_M is represented as:

$$C_c = \frac{(G_M^2 + \omega^2 C_M^2) C_M}{a^2 + \omega^2 C_M^2} \qquad (4.6.1)$$

and

$$a = G_M - (G_M^2 + \omega^2 C_M^2) R_s \qquad (4.6.2)$$

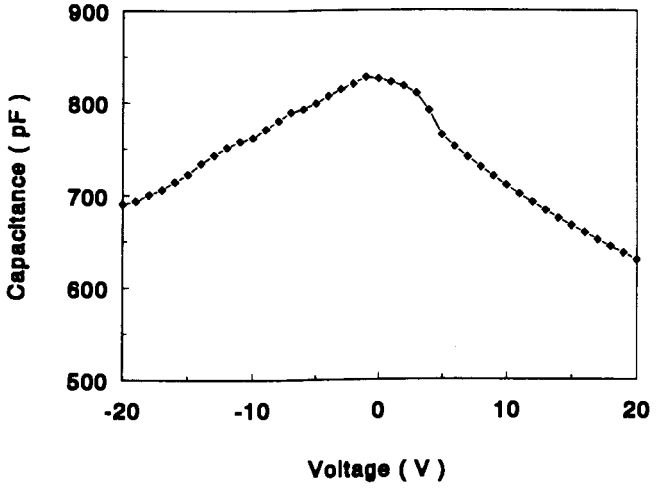

Figure 4.6.2 C–V characteristics for polymer-MIS structure at 1MHz for relatively thick film (~1μm).

Figure 4.6.2 shows the C_c–V responses for our polymer device at 1MHz for a relatively thick film (~1μm). The capacitance decreases when the applied

voltage is made more positive, but no obvious minimum capacitance is observed at high positive voltage. This behavior is similar to silicon C-V curves under deep depletion conditions. The formation of a deep depletion suggests that the minority carriers generation time is long, or the population of interface states is large. No observation of inversion layer in the polymer-MIS structure has been reported. The lack of this observation is presumedly due to the difficulties of generation of negatively charged carriers, i.e., anti-solitons, anti-polarons and antibipolarons in the depletion region and the very low migration rate of these charged carriers in the polymer. The variation of capacitance in the deep depletion regime can be modelled as [Goet66]:

$$\left(\frac{C_i}{C_c}\right)^2 - 1 = \left(\frac{C_i}{S}\right)^2 \frac{2(V - V_f)}{qN_A \epsilon \epsilon_0} \qquad (4.6.3)$$

where S is polymer–MIS diode area, N_A is approximately majority carriers concentration in polymer, C_i is insulator capacitance and V_f is the flat band potential. N_A of $4.7\times10^{16}cm^{-3}$ can be estimated from the slope of a plot $(C_i/C)^2$ as function of voltage, and V_f of $-1.8V$ can be obtained from the intercept of the same plot (Figure 4.6.3). The majority carriers value is in agreement with the carrier concentration extracted from I-V MISFET using the same polymer, i.e., $5.0\times10^{16}cm^{-3}$.

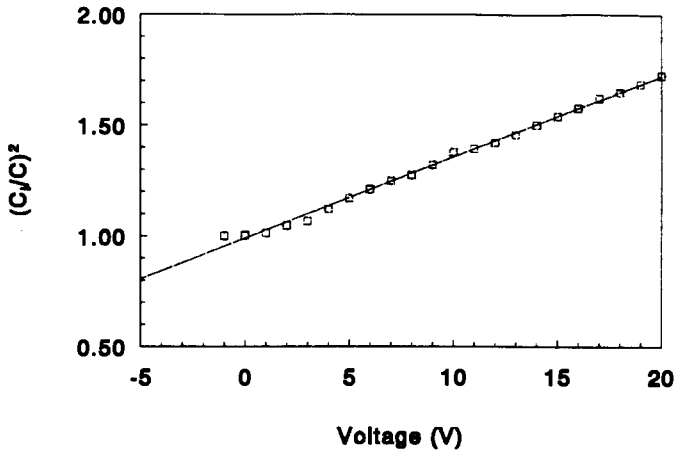

Figure 4.6.3 Variation of $(C_i/C)^2$ vs voltage biases, the majority carrier concentration can be obtained from the slope of curve.

At negative biases, it is reported [Burr89,Ziem91,Tsum88,Horo90] that the capacitance is independent of the voltage and the capacitance of the structure is approximately equal to the geometric capacitance of the insulator, C_i. This suggests the accumulation layer has a very high differential capacitance due to its very thin nature. However our C-V measurement indicate that capacitance decreased when voltage was swept more negative. We conclude that the accumulation layer for the polymer MIS structure is sufficient thick at high frequency that effects the capacitance of the MIS structure. This is the first evidence of a relative "thick" accumulation layer. We attribute it to the high purity of the polymer (see next chapter).

During the formation of accumulation layer in p-type silicon MIS structures, majority carriers (holes) are attracted to the insulator surface. The large population of majority carriers at the silicon/insulator surface is sufficient to shield the electric field, and exhibits a high differential capacitance. In semiconducting polymers, carrier movement normal to the chain direction is limited by its topological property and the carrier mobility is 10^8 orders smaller than silicon. Therefore, under high frequency signal, polarons and bipolarons can not respond quickly to the a.c. signal to screen electric field at surface. Instead of enhancement of the carrier concentration at the accumulation layer surface, the accumulation layer thickness increase in order to accommodate more carriers and thereby shield the applied electric field. In the process, the capacitance of the MIS structure at negative gate bias can be treated as an insulator capacitance C_i in series with accumulation layer capacitance C_a, which can be represented as

$$C_a = \frac{\epsilon S}{d(V)} \qquad (4.6.5)$$

ϵ is the dielectric constant, S is the MIS structure effective area. Accumulation layer thickness d(V) is dependent on gate biases: it increases with the applied negative gate bias, and its associated capacitance subsequently decreases. The actual capacitance C_c

$$C_c = \frac{C_i C_a}{C_i + C_a} \qquad (4.6.6)$$

decrease as the accumulation layer capacitance decreases, so a capacitance drop is observed when gate bias is made more negative. From above equation, accumulation layer thicknesses at 1MHz C-V measurement can be obtained and their relationship with applied gate biases is shown in Figure 4.6.4.

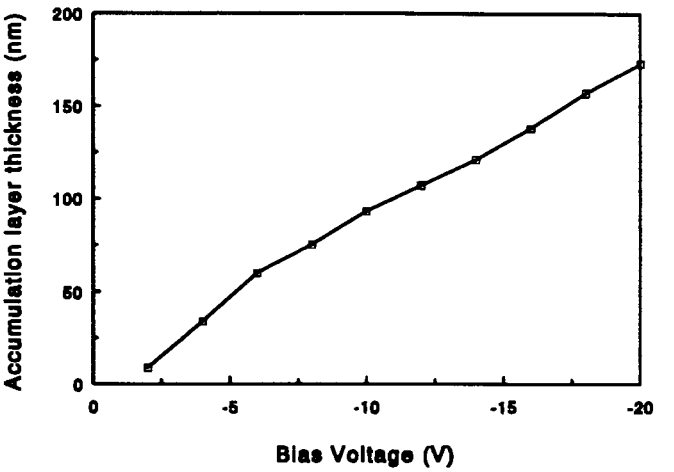

Figure 4.6.4 The accumulation layer thickness obtained from 1MHz C-V measurement versus gate biases.

In addition to the differential capacitance, the conductance variation with voltage G-V was also obtained in our MIS structure and is shown in Figure 4.6.4 . The variation conductance with voltage indicate the presence of the dissipative processes associated the charge injection precess. When capacitances drop at both voltage ends, associated discharge processes give rise to the displacement current and subsequent conductance increments. The G-V results are consistent with the C-V results.

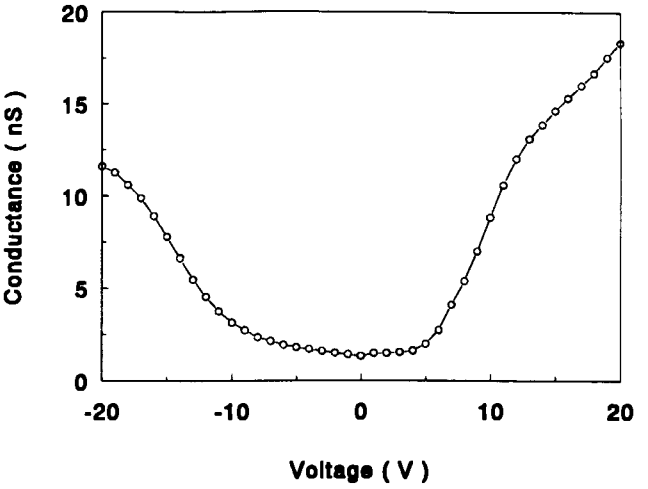

Figure 4.6.5 Conductance-voltage response for polymer-MIS structure at high frequency.

Chapter 5 Electrical Improvements on Polymer–MISFETs

5.1 Photolytic Tuning of Thick film Polymer-MISFETs

Thick film polymer MISFETs were also studied in this work. Figure 5.1.1 shows I_{DS}–V_{DS} characteristics of polymer MISFET with polymer film thickness ~ 1 μm. A large ohmic bulk current is observed, which obscures the FET characteristics. The saturation region can not be easily distinguished, but gate modulation can still be seen. The carriers mobility for this FET was determined to be $6.8 \times 10^{-4} cm^2 V^{-1} s^{-1}$ using the same methods described in the last chapter. Thick films consistently gave higher surface mobilities than thin films, and this observation is consistent with other studies [Assa88, Van91]. Figure 5.1.2 shows I_{DS}–V_{GS} characteristics of thick film MISFET. Although a thicker polymer film has larger mobility than a thin film, the channel current modulation does not show an appreciable change with the gate biases due to the large bulk current,

the channel current ratio at 0V and –30V is about 50 times smaller than the ratio for thin film MISFETs.

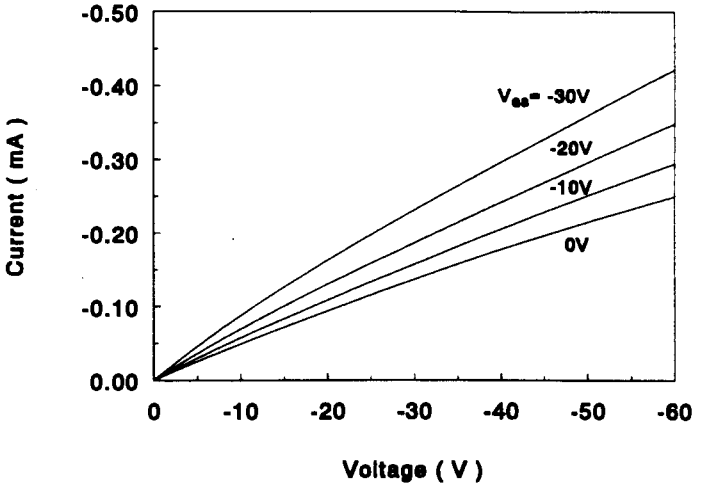

Figure 5.1.1 I_{DS}–V_{DS} characteristics of polymer–MISFET (polymer film thickness $\sim$1 μm).

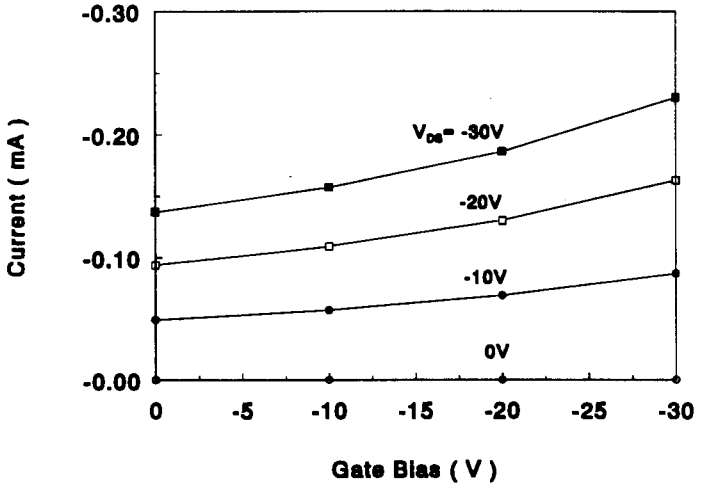

Figure 5.1.2 I_{DS}–V_{GS} characteristics of thick film MISFET (polymer film thickness $\sim$1 μm).

In an effort to fine tune MISFET electrical characteristics and eliminate the ohmic current observed for "thick film" MISFET, we utilized photochemically-induced degradation of π–conjugated polymers. The principle is shown schematically in Figure 5.1.3 and explained as follows.

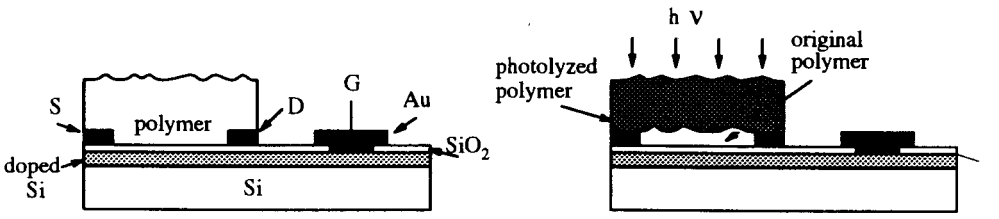

(a) (b)

Figure 5.1.3 A schematic representation of photolysis experiment on polymer-MISFET.

Poly(3–alkylthiophenes) sensitizes the generation of singlet oxygen upon exposure to UV or visible light [Abdo91]. The latter reacts with thienyl groups in the main polymer chain via a 1,4 Diels-Alder addition to break π–electron delocalization in the one dimensional chain. As a result, photolysis in the presence of oxygen results in loss of conjugation, optical bleaching and decreased electrical conductivity. A polymer MISFET was prepared using a relatively thick film of

poly(3–hexylthiophene) ($\sim$1 μm). Upon irradiation of the film with laser light (442nm, 200 mJ/cm^2), I_{DS} drops considerably and the field–effect response is observed, The extinction coefficient of the polymer at 442nm is 5480 cm^{-1}, and the density is 1.1g/cm^3 [Van91], thus the penetration depth of irradiation at a transmittance equivalent to e^{-1}, i.e. 63% of light absorbed, was 0.12μm. Upon irradiation, the bulk conductivity in the polymer is reduced by photochemical degradation from the surface down. As photolysis proceeds and the surface layer of the polymer is photobleached, the depth of penetration increases. Eventually the π–conjugated region providing ohmic, bulk conductivity is destroyed, leaving the field-active polymer layer intact. Under these conditions, FET-like response functions are observed as shown in Figure 5.1.4. Mobility before photolysis was $6.4 \times 10^{-4} cm^2 V^{-1} s^{-1}$, but decreased to $3.2 \times 10^{-4} cm^2 V^{-1} s^{-1}$ following laser irradiation. Field-effect mobilities are however an order of magnitude larger than thin film MISFETs, presumably because the former retains a π–conjugated thicker layer than 0.25 μm. This is evident from the observable ohmic current contribution to I-V curves. Irradiation of thin film (0.12μm) polymer MISFETs under the same conditions however results in lower values of I_{DS}, lower effective mobilities and generally deterioration of MISFETs. This of course is due to direct degradation of the field-active layer of the polymer substrate.

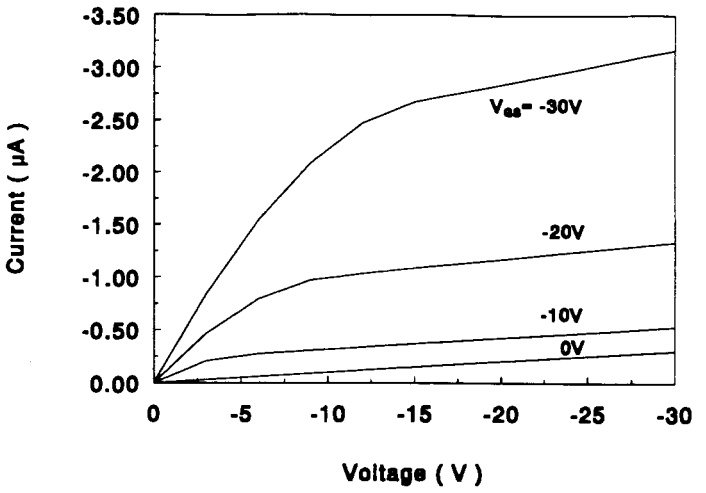

Figure 5.1.4 I_{DS}–V_{GS} characteristics of thick film MISFET ($\sim$1 μm) after photolysis.

In order to have an idea about minimum film thickness about polymer MISFET, it is important to estimate the accumulation layer thickness under different gate biases.

For p-type substrate under accumulation condition, the relationship among electrical field at interface E_s, surface potential V_s and applied gate voltage V_G are represented by [Sze81]:

$$E_s = -\sqrt{\frac{2kTN_a}{\epsilon_p}}\left[exp\left(-\frac{qV_s}{kT}\right) + \frac{qV_s}{kT} - 1\right]^{1/2} \qquad (5.1.1)$$

$$V_G = V_f + V_s + \frac{\epsilon_p E_s}{\epsilon_i} d \qquad (5.1.2)$$

where minority carriers contribution are neglected since its ratio with majority carrier is very small for the case of polymer.

Surface differential capacitance per unit area is

$$C_s = \frac{dQ_s}{dVs} = \epsilon_p \frac{dE_s}{dV_s} \qquad (5.1.3)$$

therefore,

$$C_s = \sqrt{\frac{q^2 N_a \epsilon_p}{2kT}} \left[exp\left(-\frac{qV_s}{kT}\right) - 1 \right] \left[exp\left(-\frac{qV_s}{kT}\right) + \frac{qV_s}{kT} - 1 \right]^{-1/2}$$

when $-qV_s >> kT$, C_s can be simplified as:

$$C_s = \sqrt{\frac{q^2 N_a \epsilon_p}{2kT}} exp\left(-\frac{qV_s}{2kT}\right) \qquad (5.1.4)$$

which corresponds to an accumulation layer with thickness of

$$d_a = \frac{\epsilon_p}{C_p} = \sqrt{\frac{2kT\epsilon_p}{q^2 N_a}} exp\left(\frac{qV_s}{2kT}\right) \qquad (5.1.5)$$

Using the above equation, the corresponding accumulation thicknesses under d.c. gate biases of –10V, –20V and –30V, are calculated to be 25nm, 23.4nm, 22.1 nm respectively. Under d.c. condition, carriers created by the applied electrical field possess enough relax time to accumulate at polymer/insulator surface, thus the accumulation layer thickness is considerably thinner than under high frequency condition.

5.2 Effect of Impurity Concentration on Polymer–MISFETs

It is well known that as-prepared π–conjugated polymer is p-type semiconductor due to extrinsic doping. A possible source for the doping is catalyst residues. The following experiments were designed to determine the role of catalyst residues on FET characteristics:

Poly(3-hexylthiophene) were synthesized in the Department of Chemistry by chemical oxidative-coupling using $FeCl_3$. Polymerization by chemical oxidative-coupling was performed according to the procedure described by Sugimoto et al. The solid product was filtered, washed successively with NH_4OH (28%), water and finally with acidified methanol. The crude polymer was dissolved in hot dichloromethane and insoluble products were removed by filtration. Low molecular weight products were removed by cooling the filtrate and adding methanol. The precipitate was filtered and dried under reduced pressure at 50°C. A fraction of the sample was purified further by soxhlet extraction using methanol (2 days) and acetone (5 days). Subsequently, a fraction of this polymer was purified even further treating a solution of the polymer in $CHCl_3$ with NH_4OH (28%). The polymer was precipitated, washed to chloride-free waste and dried as described above. By this route three polymers samples containing various levels of iron impurities were obtained.

Iron content was determined by a standard acid digestion procedures followed

by atomic absorption detection. Dissolution of iron and break down the organic materials was achieved by digesting 50 mg of polymer with 10 mL of concentrated sulfuric and nitric acids (50 vol%). Stock solutions of iron was prepared by dissolving 0.250 g of iron (Baker Chemicals) in 250 mL nitric acid (~5mL) and distilled water. Standard iron solutions (25mL) containing 2, 4, 8, 12, 16 and 20 ppm iron were prepared by appropriate dilution with 0.1 HCl.

Polymers prepared with different dopant levels were used for devices fabrication. Figure 5.2.1 (a),(b),(c) show the I_{DS}-V_{DS} curves of MISFETs based on polymers prepared by oxidative coupling techniques. Residual iron concentrations in polymer were determined to be (a) 3.2%, (b) 1.32% and (c) 0.05% respectively.

Mobility and conductivity for different polymer MISFET were extracted using the same methods as described in chapter 4: The conductivity was extracted at zero gate bias; the mobility was obtained at gate bias of –30V and V_{DS} of 5V. The mobility and conductivity values are listed in Table 5.2.1. The majority carriers concentration in the MISFET were also estimated. As the external impurity concentration in polymer decrease, the bulk ohmic currents, and the FET gate bias modulation correspondingly increase.

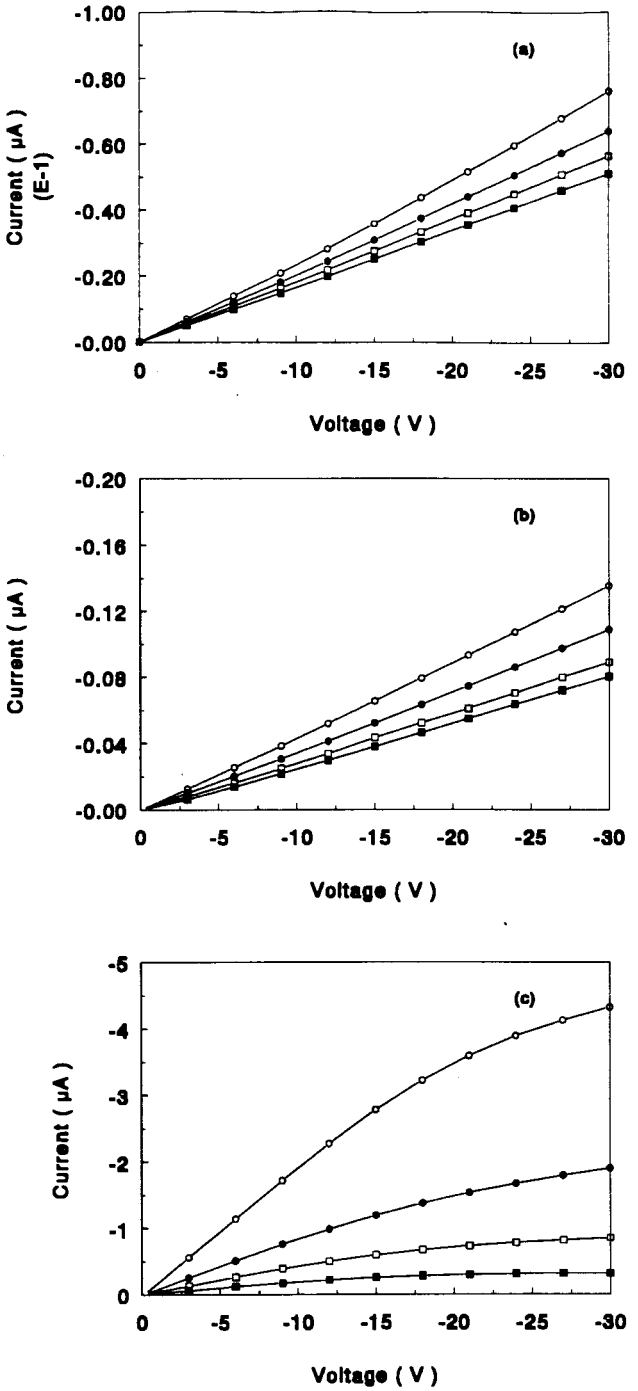

Figure 5.2.1 I_{DS}-V_{DS} curves of MISFETs based on polymers with varying degrees of iron salt impurity. The iron contents for top, middle, and bottom polymers are 3.2%, 1.32%, and 0.05% respectively.

Table 5.2.1 The mobilities, conductivities and carrier concentrations of polymer-MISFETs fabricated with polymers of different iron dopant levels.

Iron Contents (wt%)	μ ($cm^2V^{-1}s^{-1}$)	σ (Scm^{-1})	n (cm^{-3})
#1 (3.2%)	6.4×10^{-8}	3.7×10^{-9}	5.8×10^{17}
#2 (1.32%)	8.4×10^{-7}	1.4×10^{-8}	1.7×10^{17}
#3 (0.05%)	2.3×10^{-5}	1.2×10^{-7}	5.1×10^{16}

These experiment results verify that impurities play an important role in carrier transport. The existence of external impurities create topographical defects in polymer. Soliton, polaron and bipolaron excitations associated with these defect increase carrier concentration, but carriers concentration does not vary linearly with impurity concentration. Presumably, impurities provide extrinsic carriers in addition to intrinsic carriers which are created by the application of electric field. These impurity ions residing in polymer are virtually immobile and attached to polymer chain end [Burr88]. Carrier movement near the surface is scattered by these impurities, thus the carrier mobility is greatly reduced due to the impurity scattering. Since mobilities increase with the decreasing impurity levels, it is concluded that polymer with low impurity concentrations are more suitable for MISFET. In addition, the bulk current is substantially enhanced due to the increase of conductivity, which arises from large enhancement of mobility at low impurity level.

5.3 Encapsulation of Polymer-MISFETs

Conducting polymers are very sensitive to oxygen, light and moisture. As a consequence polymer-MISFETs have limited stability when exposed to ambient atmosphere for long periods. Passivation layers on the top of polymer-MISFET seem to provide a satisfactory solution.

Figure 5.3.1 show a typical I_{DS}–V_{DS} curves for thin film P3HT MISFET upon exposure to air for four days. This should be compared to the I_{DS}–V_{DS} response of the pristine FET (Figure 4.4.2). It is observed that FET characteristics degrade substantially in air, the FET bulk current becomes large, and gate bias modulation becomes poor.

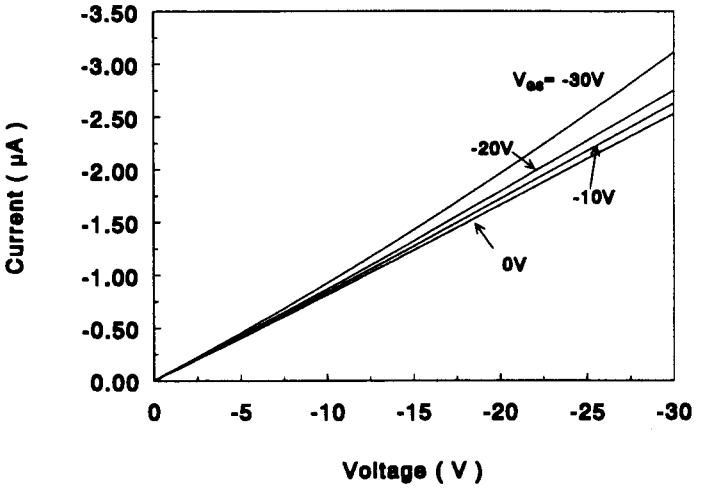

Figure 5.3.1 I_{DS}–V_{DS} curves for thin film P3HT-MISFET upon exposure to air for four days

The electrical performance of a pristine polymer-MISFET was monitored for a week. A plot of mobility and conductivity variation with time was shown in Figure 5.3.2. This change in FET response reflects the ability of molecular oxygen to act as a weak oxidant/dopant for the polymer, this observation is consistent with studies of poly(3–methylthiophene). In addition, the possibility of light and moisture with polymer structure leads to further complications, at present this part of research has been done in our studies.

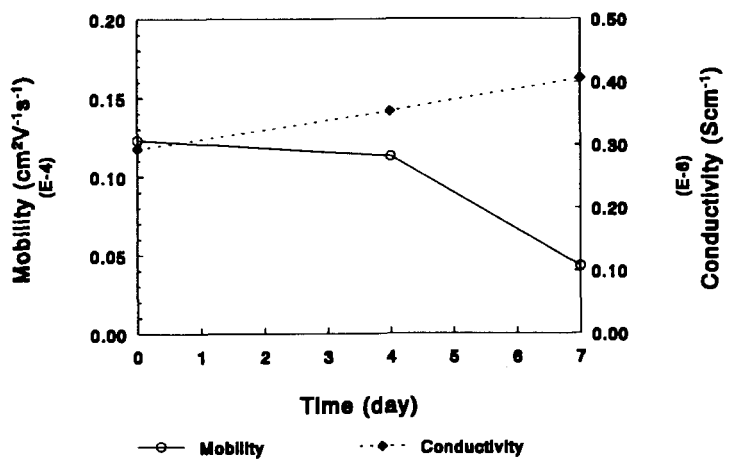

Figure 5.3.2 Variation of mobility and conductivity with time upon exposure to air.

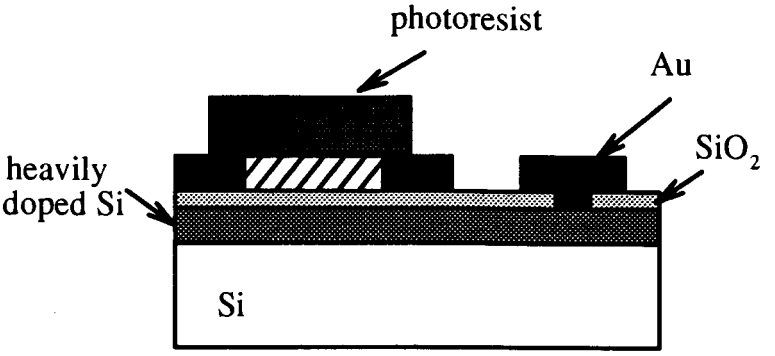

Figure 5.3.3 Schematic representation of a polymer MISFET encapsulated with a photoresist layer.

In order to protect the polymer film from the atmosphere, a layer of photoresist was spin-cast onto the polymer-MISFET following device fabrication. Laser direct writing was used to photolithographically pattern the photoresist to uncover the source, drain and gate contacts. The photoresist layer was postbaked in air for 30 minutes to remove residual solvents, cure the photoresist surface layer, and suppress its photochemical reactivity. The modified polymer MISFET structure is shown in Figure 5.3.3.The encapsulated P3HT MISFETs were monitored two months. I-V responses following postbaking of the photoresist, and exposed in air for 1day, 15days and 60 days are shown in Figure 5.3.4. The change in mobility and conductivity with time are shown in Figure 5.3.5. Note that the mobility

decreased by ~60% after encapsulation. This suggests that the photoresist introduces minor changes to the underlying polymer film. Chemical analysis indicates two main sources for these changes: First, introduction of defects in the polymer film. This is attributed to swelling of the polymer due to the fact that the photoresist contains xylene as one of its components which is a good solvent for the polymer. Second, baking of the photoresist induces thermal decomposition of one of the photoresist active component namely diazonaphthoquinone which might introduce some impurities in the polymer film [Abou93]. Carrier mobility for passivated FETs, however, increases with time and reaches steady state. This implies enhanced chemical and electrical stability of the device compared to non-passivated FETs.

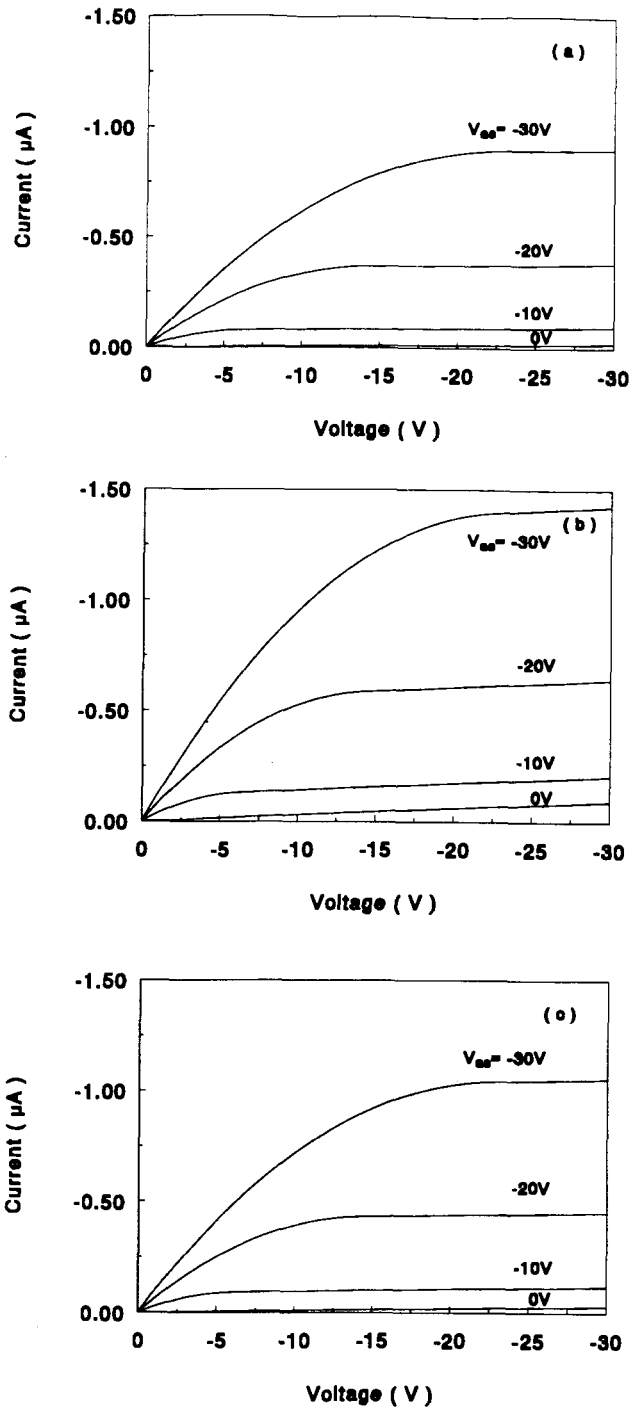

Figure 5.3.4 Typical I-V response of encapsulated polymer-MISFET exposed to air for (a) 1day, (b) 15days and (c) 60 days.

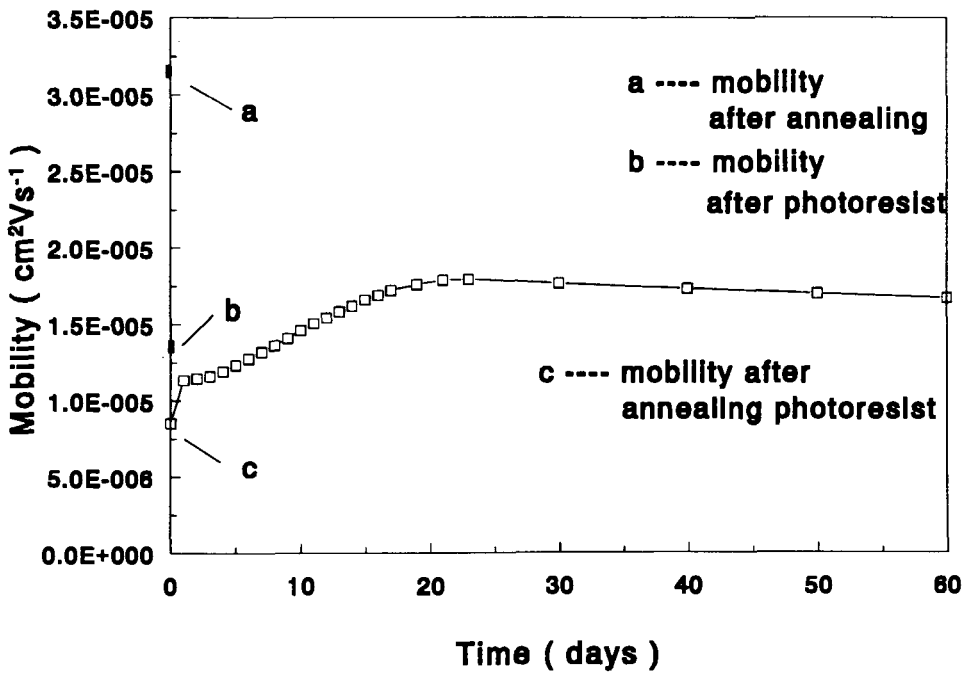

Figure 5.3.5 Variation of mobility and conductivity with elapsed time after photoresist passivation. and exposed to air. (a) mobility just after annealing polymer-MISFET; (b) mobility just after applying photoresist on annealed polymer-MISFET; (c) mobility after annealing photoresist.

Chapter 6 Conclusions

In our research, we have fabricated MISFETs based on the semiconducting polymer, poly(3–hexylthiophene). We have developed an equivalent circuit of these polymer-based MISFETs, and have obtained very good agreement between simulations based on the circuit model and experimental results. We concentrate on describing current-voltage characteristics of MISFETs since the FET structure is ideal for studying the electrical field dependence of carriers in the polymers. Our current experimental results on mobility and transconductance are dependent on film thickness, but are significantly lower than that of silicon-based FETs. We expect that this gap will be narrowed as the technology matures through improved understanding of the structure-property relationships of semiconducting π–conjugated polymers. We have also investigated capacitance-voltage characteristics of P3HT MIS structure, A conventional depletion region occurs at positive voltage, and accumulation layer capacitances were observed at negative voltage.

In addition, we have shown for the first time how the thickness of the substrate can be tuned by photolysis; that passivation can stabilize the electrical performance of polymer MISFET; and that impurities affect the performance of polymer-MISFETs. By utilizing this knowledge, electrical improvements of higher carrier mobility, low substrate current, and stability of polymer-based FET has been realized.

Chapter 7 References

[Abdo91] M.S.A. Abdou, M.I. Arroyo, G. Diaz-Quijada, & S. Holdcroft. "Photoimaging of Electronically Conducting Polymer Networks", *Chem. Mater.* **3**, 1003 (1991)

[Abdo92] M.S.A. Abdou, Z.W. Xie, A.M. Leung and S. Holdcroft. "Laser, Direct-Write Microlithography of Soluble Polythiophene", *Synth. Met.* **in press** (1992)

[Abdo93] M.S.A. Abdou and S. Holdcroft. "Mechanism of Photodegration of Poly(3–alkylthiophene) in Solution", *Macromolecules*, **26**, 2594 (1993)

[Abdou] M.S.A. Abdou, Y.Son and S. Holdcroft. *unpublished results* (1993)

[Assa88] A. Assadi, C. Svensson, M. Willander & O. Inganas. "Field Effect Mobility of Poly(3–hexylthiophene)", *Appl. Phys. Lett.* **53**, 195 (1988)

[Braz81] S.A. Brazovskii & N.Kirova, "Excitons, Polarons and Bipolarons in Conducting Polymers", *Sov. Phys. JETP lett.* **33**, 4 (1981).

[Burr88] J.H. Burroughes, C.A.Jones and R.H. Friend. "New Semiconductor Device Physics in Polymer Diodes and Transistors", *Nature*, **335**, 137 (1988)

[Burj89] J.H Burroughes, C.A.Jones and R.H. Friend. "Polymer Semiconductor Devices", *Synth. Met.* , **28**, 735 (1989)

[Burr89] J.H Burroughes, R.H. Friend and P.C. Allen. "Field-Effect Conductivity in Polyacetylene— Construction of a field-effect transistors", *J. Phys. D Appl. Phys.*, **22**, 956 (1989)

[Burr90] J.H. Burroughes, D.D.C. Bradley, A.R. Brown, R.N. Marks, K. Mackay, R.H. Friend, P.L. Burns, & A.B. Holmes. "Light-Emitting Diodes Based on Conjugated Polymers", *Nature*, **347**, 539 (1990)

[Burr91] J.H. Burroughes, D.D.C. Bradley, A.R. Brown, R.N. Marks, K. Mackay, R.H. Friend, P.L. Burns, & A.B. Holmes. "Light-Emitting Diodes Based on Conjugated Polymers", *Nature*, **347**, 539 (1990)

[Camp81] D.K.Campbell & A.R.Bishop, "Solitons in Polyacetylene and the Relativistic Field Theory Model", *Phys. Rev.* **B24**, 4859 (1981).

[Chia77] C.K.Chiang, C.R.Fincher, Jr., Y.M.Park, A.J.Heeger, H.Shirakawa, E.J.Loius, S.C.Gau, and A.G. MacDiarmid, "Electrical Conductivity in Doped Polyacetylene", *Synth. Met.* **1**, 175 (1980).

[Chia78] C.K. Chiang, M.A. Druy, S.C. Gau, A.J. Heeger, E.J. Louis, A.G. MacDiarmid, Y.W. Park, H. Shirakawa. *J Am. Chem. Soc.* **100**, 1013 (1978)

[Epst81] A.J.Epstein, H.Rommelmann, M.Abkowitz, and H.W.Gibson, " Anomalous Frequency-Dependent Conductivity of Polyacetylene", *Phys. Rev. Lett.*, **47**, 1549 (1981)

[Fich89] D.Fichou, G.Horowitz, Y.Nishikitani, & F.Garnier. "Semiconducting Conjugated Oligomers for Molecular Electronics", *Synth. Met.* **28**, (1989)

[Frie87] R.H.Friend, D.D.C.Bradley and P.D.Townsend, "Photoexcitation in Conjugated Polymers", *J. Phys. D: Appl. Phys.*, **20**, 1367 (1987)

[Garn87] F. Garnier, & G. Horowitz. "Organic Semiconducting Polymers as Conjugated Oligomers for Molecular Electronics", *Synth. Met.* **18**, 693 (1987)

[Garn89] F.Garnier, G.Horowitz and D.Fichou "Conjugated Polymers and Oligomers as active material for electronic devices", *Synth. Met.* **28**, 705 (1989)

[Garn90] F. Garnier, G. Horowitz, X. Peng & D. Fichou. "Thin Film Transistors Based on Alpha Conjugated Oligomers", *Adv. Mater.*, **2**, 592 (1990)

[Glen89] S. Glenis, & A.J. Frank. "Schottky Barrier Formation Between Poly(3–methylthiophene) and n-type Cadmium Sulfide", *Synth. Met.* **28**, C681 (1989)

[Gran92] M. Granstrom, O. Inganas. "A kinetic Study of Thermal Doping in the Poly(3–alkylthiophene), *Synth. Met.* **48**, 21 (1992)

[Gros74] D.J.Gross & A.Neveu, " Dynamical Symmetry Breaking in Asymptotically Free Field Theories", *Phys. Rev.* **D10**, 3235 (1974)

[Gust91] G.Gustafasson, O.Inganas, M.Sundberg and C.Svensson, "Rectifying Metal/Poly(3–hexylthiophene) Contacts",*Synth. Met.* **41–43**, 499 (1974)

[Heeg91] Alan.J.Heeger and Paul Smith, "Conjugated Polymers" 141–210, 1991 Kluwer Academic Publishers.

[Hold91] S. Holdcroft. "Photochain Scission of Soluble Electrochemically Conjugated Polymer: Poly(3–hexylthiophene)", *Macromolecules* **24**, 2119 (1991)

[Hold91–2] S. Holdcroft. "A photochemical Study of Poly(3–hexylthiophene)", *Macromolecules* **24**, 4834 (1991)

[Hold91–3] S. Holdcroft. "Determination of Molecular Weight and MarkHouwink Constants for Soluble Electronically Conducting Polymers", *J. Polym. Sci. Polym. Phys.* **29**, 1585 (1991)

[Horo91] G. Horowitz, D. Fichou, X. Peng & F. Garnier. "Field-effect Mobility on Poly(3–hexylthiophene), *Synth. Met.* **41**, 1127 (1991)

[Ito74] T. Ito, H.Shirakawa, S.Ikeda. "Simultaneous Polymerization and Formation of Polyacetylene Film on the Surface of Concentrated Soluble Ziegler Type Catalyst Solution", *J. Polym. Sci. Polym. Chem.* **12**, 11 (1974).

[Kive81] S.Kivelson, "Electron Hopping Conduction in the Soliton Model of Polyacetylene", *Phys. Rev. Lett.* **46**, 1344 (1981).

[Koez87] H. Koezuka, A. Tsumura & T. Ando. "Field Effect Transistor Utilizing Conducting Polymer", *Synth. Met.* **18**, 699 (1987)

[Mark62] Mark.P, Helfrich.W, *J. Appl. Phys.* **33** No.1 (1962)

[More] W.M.Moreau. "Semiconductor Lithography", Plenum Press, New York. 1988.

[Ohmo91] Yoshihiko Kanemitsu, Hiroshi Funada, and Yasuaki Masumoto "Electric Field Dependence of Hole Drift Mobility in Molecularly Doped Polymers: Importance of the Disorder of the Hopping Sites", *J. Appl. Phys.* **30** No.4A, 610 (1991)

[Park80] Y.W.Park, A.J.Heeger, M.A.Druy, and A.G.macDiarmid, " Electrical Transport in Doped Polyacetylene", *J. Chem. Phys.* **73**, 946(1980).

[Polo91] J.Paloheimo, H.Stubb, P.Yli-Lahti and P.K.Uivalainene, "Field-Effect Conduction in Polyalkylthiophene", *Synth. Met.* **41–43**, 563 (1991).

[Rice79] M.J.Rice, "Charged π–Phase Kinks in Lightly Doped Polyacetylene", *Phys.Lett.* **71A**, 152–154 (1979).

[Sugi86] R. Sugimoto, S. Takeda, H.B. Gu, & K. Yoshino. *Chem. Express* **1**, 635 (1986)

[Suwp79] W.P.Su, J.R.Schrieffer, and A.J.Heeger, "Solitons in Polyacetylene", *Phys. Rev. Lett.* **42**, 1698 (1979).

[Suwp80] W.P.Su, J.R.Schrieffer, and A.J.Heeger, "Soliton Excitations in Polyacetylene", *Phys. Rev.* **B22**, 2099–2111 (1980).

[Suzu80] N.Suzuki, M.Ozaki, S.Etemad, A.J.Heeger, and A.G. MacDiarmid, "Solitons in Polyacetylene: Effects of Dilute Doping on Optical Absorption Spectra", Phys. Rev.Lett. 45 1209–1213 (1980).

[Sze81] S.M. Sze. "Physics of Semiconductor Devices", 2nd Edition. John Wiley & Sons, Inc. 1981.

[Taka91] T. Taka, M.T. Loponen, J. Laasko, K. Suuronen, P. Valkeienen, J.E. Osterholm. "Degradation Studies of Doped and Dedoped Poly(3–octylthiophene), *Synth. Met.* **41–43**, 567 (1991)

[Tayl91] D.M Taylor, H.L Gomes, A.E. Underhill, S. Edge, and P.I. Clemonson. "Effect of Oxygen on the Electrical Characteristics of Field Effect Transistors Formed from Electrochemically Deposited Films of Poly(3–methylthiophene), *J. Phys. D: Appl. Phys.* **24**, 2032 (1991)

[Tomo87] H. Tomozawa, D. Braun, S. Philips, A.J Heeger & H. Kroemer. *Synth. Met.* **22**, 63 (1987)

[Tomo89] H. Tomozawa, D. Braun, S.D. Philips, R. Worland, A.J. Heeger, & H. Kroemer. "Metal-Polymer Schottky Barriers on Cast Films of Soluble Poly(3–alkylthiophene)"*Synth. Met.* **28**, C687 (1989)

[Town87] P.D.Townsend and R.H.Friend, "Photoexcitation in Oriented Polyacetylene", *Synth. Met.*, **17**, 361 (1987).

[Van91] R.H.M. van der Leur, B. de Ruiter. "Dielectric Properties of Poly(3–hexylthiophene) Powder", *Synth. Met.*,**44**, 327 (1991)

[Wang86] C.L. Wang, Z.B. Su, F. Martino. "Bipolaron Dynamics in Nearly Degenerate Quasi-one-dimensional Polymers", *Phys. Rev.* **B33**, 1512 (1986)

[Wang91] Y. Wang, M.F. Rubner. *Polymer Preprints* **31**, 402 (1991)

[Wein79] B.R.Weinberger, J.Kaufer, A.J.Heeger, A.Pron, and A.G.MacDiarmid, "Magnetic Susceptibility of Doped Polyacetylene", Phys. Rev. B20, 223–230 (1979).

[Wuwp88] W.P. Wu, J.R. Schrieffer and A.J. Heeger. "Soliton Excitation in Polyacetylene", *Phys. Rev.* **B28**, 2388 (1988)

[Yosh91] K. Yoshino, K. Keneto, & S. Takeda. "Electric Field Dependence of Hole Drift Mobility in Molecularly Doped Polymers: Importance of the Disorder of the Hopping Sites", *J. Appl. Phys* **71**, 300, 1991.

[Zuo89] Z.P. Zuo, M.J. Deen and J. Wang. *Proceeding of the Canadian Conference on Electrical and Computer Engineering*, Montreal. Sept. 1989. Edited by V.K. Bhargava.

APPENDIX I

THIS IS THE SPICE FILE FOR THIN FILM (0.25μm) POLYMER MISFET

```
* This model treat polymer MISFET as combination of ordinary normally-off
*MISFET and varistor.
* D=1 G=2 S=0
.MODEL MPOLY PMOS VTO=0 TOX=1U UO=3.6e-5 LAMBDA=5e-3
M1 4 2 5 0 MPOLY L=10U W=4000U
R1 0 1 2.4E10
.DC V1 0 -60 -2
R2 5 0 1K
R3 1 4 1K
V1 1 3
V2 2 0 DC -30
VI1 3 0
.WIDTH OUT=80
.PRINT DC I(VI1)
.PLOT DC I(VI1)
.END
```

```
* This model treat polymer MISFET as combination of ordinary normally-off
*MISFET and varistor.
* D=1 G=2 S=0
.MODEL MPOLY PMOS VTO=0 TOX=1U UO=2.5e-5 LAMBDA=5e-3
M1 4 2 5 0 MPOLY L=10U W=4000U
R1 0 1 2.4E10
.DC V1 0 -60 -2
R2 5 0 1K
R3 1 4 1K
V1 1 3
V2 2 0 DC -20
VI1 3 0
.WIDTH OUT=80
.PRINT DC I(VI1)
.PLOT DC I(VI1)
.END
```

```
* This model treat polymer MISFET as combination of ordinary normally-off
*MISFET and varistor.
* D=1 G=2 S=0
.MODEL MPOLY PMOS VTO=0 TOX=1U UO=3e-5 LAMBDA=5e-3
M1 4 2 5 0 MPOLY L=10U W=4000U
R1 0 1 2.4E10
.DC V1 0 -60 -2
R2 5 0 1K
R3 1 4 1K
V1 1 3
V2 2 0 DC -10
VI1 3 0
.WIDTH OUT=80
.PRINT DC I(VI1)
.PLOT DC I(VI1)
.END
```

APPENDIX II

THIS IS THE SPICE FILE FOR THICK FILM (1μm) POLYMER MISFET

```
* This model treat polymer MISFET as combination of ordinary normally-off
*MISFET and varistor.
* D=1 G=2 S=0
.MODEL MPOLY PMOS VTO=0 TOX=1U UO=3.6E-4 LAMBDA=0.019
M1 4 2 5 0 MPOLY L=10U W=4000U
R1 0 1 3.3E8
.DC V1 0 -60 -2
R2 5 0 0.2K
R3 1 4 0.2K
V1 1 3
V2 2 0 DC -30
VI1 3 0
.WIDTH OUT=80
.PRINT DC I(VI1)
.PLOT DC I(VI1)
.END
```

```
* This model treat polymer MISFET as combination of ordinary normally-off
* MISFET and varistor.
* D=1 G=2 S=0
.MODEL MPOLY PMOS VTO=0 TOX=1U UO=2.8e-4 LAMBDA=0.034
M1 4 2 5 0 MPOLY L=10U W=4000U
R1 0 1 3.3E8
.DC V1 0 -60 -2
R2 5 0 0.2K
R3 1 4 0.2K
V1 1 3
V2 2 0 DC -20
VI1 3 0
.WIDTH OUT=80
.PRINT DC I(VI1)
.PLOT DC I(VI1)
.END
```

```
* This model treat polymer MISFET as combination of ordinary normally-off
* MISFET and varistor.
* D=1 G=2 S=0
.MODEL MPOLY PMOS VTO=0 TOX=1U UO=3.2e-4 LAMBDA=0.050
M1 4 2 5 0 MPOLY L=10U W=4000U
R1 0 1 3.3E8
.DC V1 0 -60 -2
R2 5 0 0.2K
R3 1 4 0.2K
V1 1 3
V2 2 0 DC -10
VI1 3 0
.WIDTH OUT=80
.PRINT DC I(VI1)
.PLOT DC I(VI1)
```